University of Alberta

NUMERICAL SIMULATION OF WIND IN PLANT CANOPIES

By

Denis Joseph Jean-Paul Pinard ©

A thesis submitted to the Faculty of Graduate Studies and Research in partial fulfillment of the requirements for the degree of Master of Science

Department of Earth and Atmospheric Sciences

Edmonton, Alberta

Fall 2000

National Library of Canada
Acquisitions and Bibliographic Services
395 Wellington Street
Ottawa ON K1A 0N4
Canada

Bibliothèque nationale du Canada
Acquisitions et services bibliographiques
395, rue Wellington
Ottawa ON K1A 0N4
Canada

Your file Votre référence

Our file Notre référence

The author has granted a non-exclusive licence allowing the National Library of Canada to reproduce, loan, distribute or sell copies of this thesis in microform, paper or electronic formats.

The author retains ownership of the copyright in this thesis. Neither the thesis nor substantial extracts from it may be printed or otherwise reproduced without the author's permission.

L'auteur a accordé une licence non exclusive permettant à la Bibliothèque nationale du Canada de reproduire, prêter, distribuer ou vendre des copies de cette thèse sous la forme de microfiche/film, de reproduction sur papier ou sur format électronique.

L'auteur conserve la propriété du droit d'auteur qui protège cette thèse. Ni la thèse ni des extraits substantiels de celle-ci ne doivent être imprimés ou autrement reproduits sans son autorisation.

0-612-60486-1

Canada

University of Alberta

Library Release Form

Name of Author: Denis Joseph Jean-Paul Pinard

Title of Thesis: NUMERICAL SIMULATION OF WIND IN PLANT CANOPIES

Degree: Master of Science

Year this Degree Granted: 2000

Permission is hereby granted to the University of Alberta Library to reproduce single copies of this thesis and to lend or sell such copies for private, scholarly or scientific research purposes only.

The author reserves all other publication and other rights in association with the copyright in the thesis, and except as herein before provided, neither the thesis nor any substantial portion thereof may be printed or otherwise reproduced in any material form whatever without the author's prior written permission.

Lot 115 Judas Creek Drive
Marsh Lake
P.O. Box 3853
Whitehorse, Yukon
Y1A 5M6

May 3/2000

University of Alberta

Faculty of Graduate Studies and Research

The undersigned certify that they have read, and recommend to the Faculty of Graduate Studies and Research for acceptance, a thesis entitled NUMERICAL SIMULATION OF WIND IN PLANT CANOPIES submitted by Denis Joseph Jean-Paul Pinard in partial fulfillment of the requirements for the degree of MASTER OF SCIENCE.

John D. Wilson

Gerhard W. Reuter

Peter M. Steffler

2 May/2000

Abstract

Wind flow through several different plant canopies (a coniferous forest, a maize crop, and two artificial wind tunnel "crops") is computer-simulated using a simple first-order closure (eddy diffusivity $K \propto \lambda\sqrt{k}$, where k is the turbulent kinetic energy, and λ is a turbulence length scale). Simulations are compared against observations, and against earlier simulations (using second-order closure) described by Katul and Chang (1999). The variables of interest include the mean horizontal wind speed $\overline{u}$, the shear stress $\overline{u'w'}$, and the turbulent kinetic energy k, all of which vary with height z in the canopy.

The drag coefficient, an important parameter in canopy flow modelling, is calculated from the Duke Forest measurements and applied in flow simulations. Results show that the mean wind speed, shear stress and turbulent kinetic energy given by the first-order closure compare well with the measured flow and with the second-order models.

Acknowledgement

I would like to thank Kerry Anderson, Richard Carr, and Peter Englefield at the Northern Forestry Centre for helping me on my experimentation with the wind flow model RAMS.

As regards financial assistance, I would like to thank the Natural Sciences and Engineering Research Council of Canada (for funding through John D. Wilson), and the University of Alberta for a graduate teaching assistantship.

Many thanks go to the staff of the department of Earth and Atmospheric Sciences and the Faculty of Graduate Studies and Research at the University of Alberta for the kind help given to me during the period of my thesis work.

My gratitude goes especially to John D. Wilson for his belief in me, his dedication and his persistent guidance, which he has kindly given to me during the course of my graduate studies.

Table of Contents

1 INTRODUCTION 1

1.1 The Study by Katul and Chang (1999) 3
1.2 A Puzzle in Katul and Chang (1999) 5
1.3 Objectives 7

2 THE PLANETARY BOUNDARY LAYER 8

2.1 Turbulent Momentum Transfer 10
2.2 Characterising Turbulence 13
2.3 The Atmospheric Surface Layer 14
2.3.1 General Wind Profile in the surface layer of the PBL 15
2.3.2 Wind Flow in a Canopy 16

3 GOVERNING EQUATIONS 19

3.1 Co-ordinate System 19
3.2 Conservation Equations under Boussinesq Approximation 20
3.2.1 Conservation of Mass 20
3.2.2 Conservation of Momentum 21
3.2.3 Conservation of Heat 22
3.3 Reduction of Conservation Equations to Reynolds Equations 22
3.3.1 Time Averaging 22
3.3.2 Applying Averaging to Conservation Equations 23
3.3.3 Turbulent Kinetic Energy 24
3.4 Applying the Reynolds Equations to Canopy Flow 26
3.4.1 Specialisation to Canopy Flow 26
3.4.2 Need for Spatial Averaging 27
3.4.3 Other Equations for the Horizontally Uniform Plant Canopy 29
3.5 Drag Coefficient 30
3.5.1 Height Variable Drag Coefficient 30
3.5.2 Height Averaged Drag Coefficient 35
3.5.3 Bulk Drag Coefficient 37

4 TURBULENCE CLOSURES 40

4.1 K-theory and the Canopy Flow Model of Wilson et al (1998) 40
4.1.1 Length Scale 41
4.1.2 TKE Dissipation Rate 43
4.2 Higher-Order Closures 43
4.2.1 Wilson and Shaw (1977) 44
4.2.2 Wilson (1988) 45

5 NUMERICAL METHOD USED TO IMPLEMENT THE K-THEORY MODEL 46

5.1 SIMPLE: Discretisation with Respect to Control Volumes 46
5.2 Staggered Grid 47
5.3 Boundary conditions 49
5.3.1 Top 49
5.3.2 Bottom 49
5.4 Investigation of Model Convergence and Grid-Independence 49
5.4.1 Grid Size Optimisation 49
5.4.2 Iteration number Optimisation 51

6 COMPARISON OF NUMERICAL WITH EXPERIMENTAL DATA AND WITH OTHERS' CALCULATIONS 53

6.1 REVISITING AND INDEPENDENTLY CHECKING THE WILSON ET AL. (1998) FIRST ORDER CLOSURE MODEL 54

6.2 COMPARING THE FIRST ORDER MODEL TO DUKE FOREST OBSERVATIONS AND SIMULATIONS FROM KATUL AND CHANG (1999) 60

7 CONCLUSIONS 67

8 REFERENCES 69

List of Tables

Table 1-1: Calculation of TKE (k) for the Duke Forest from the measured velocity standard deviations cited in KC99 Table 3. 6

Table 3-1: Measured mean winds, shear stress, and leaf area density in the Duke Forest of KC99. The drag coefficients C_d and C_{dp} have been calculated based on the given Duke Forest data, using Equation (3.23, 3.24). The five numbers in italics in the $a(z)$ column are interpolated data. 32

Table 3-2: Data for derivation of a height-independent drag coefficient for the Duke Forest (h_c = 14 m). (KC99 provide $\overline{u}/u_*$ and $a(z)$) The first three columns are used to calculate the height averaged drag coefficient $\overline{C_d}$ = 0.2. The last column shows the height variable $\overline{C_d}\,ah$ using column $a(z)$ multiplied by $\overline{C_d}$ = 0.2. 36

Table 3-3: Measured $\overline{u}/u_*$ profile is used to calculate C_{db} using Equation 3.32. 38

Table 6-1: Parameters of the Duke Canopy Experiments 61

List of Figures

Figure 1-1: Comparing the contradicting values for normalised TKE given by KC99..6
Figure 2-1: Daytime profiles of mean potential temperature and mean horizontal velocity through the PBL 8
Figure 2-2: A hypothetical laminar flow 11
Figure 2-3: Fluctuations u' and w' in horizontal and vertical velocity 13
Figure 2-4: Schematic profiles of the principal wind and turbulence statistics 18
Figure 3-1: Co-ordinate system in a canopy flow 19
Figure 3-2: Measured values of normalised wind statistics in Duke Forest 34
Figure 3-3: As seen here, C_{db} is calculated as the reciprical of the total area 38
Figure 3-4: The drag coefficient $C_{dp}(z)$ is negative at the ground and 39
Figure 4-1: The length scale in a canopy such as the Duke Forest 42
Figure 5-1: Control volumes and grid point layout for discretised model 48
Figure 5-2: Sensitivity of modelled profile of mean wind to grid spacing 50
Figure 5-3: Using mean wind speed values at height $z/h_c = 0.5$ from Figure 5-2 51
Figure 5-4: The normalised mean wind profile with 100 grid points in the canopy 52
Figure 5-5: More specific depiction of convergence in speed values 52
Figure 6-1: New simulations (with first-order closure) for the Furry Hill 55
Figure 6-2: New simulations (with first-order closure) for the Elora maize 56
Figure 6-3: New simulations (with first-order closure) for the Tombstone canopy 57
Figure 6-4: In the original Wilson et al (1998) simulation of Tombstone 59
Figure 6-5: Mean wind speed $\overline{u}$ of the first order model against observed 62
Figure 6-6: The shear stress $\overline{u'w'}$, from the first order model against observed 63
Figure 6-7: The turbulent kinetic energy k of the first order model against observed..64
Figure 6-8: Reproduced from KC99 these are their charts of their modelled 66

List of Symbols and Abbreviations

K	Eddy viscosity, turbulent transport coefficient. Turbulence closure in the conservation equations. [m^2s^{-1}]
k, TKE	Turbulent kinetic energy. [m^2s^{-2}]
ASL	Atmospheric surface layer.
PBL	Planetary boundary layer.
PT_t	Pressure and turbulent transport. [m^2s^{-3}]
x, y, z	Co-ordinates in a three-dimensional system. [m]
z_o	The surface roughness length.[m]
u, v, w	Wind speed corresponding to x, y, z. [ms^{-1}]
u_i	Vector velocity, $u_i = \vec{u} = u_1, u_2, u_3 = u, v, w$. [$ms^{-1}$]
u' , v' , w'	Fluctuations of the wind speeds. [ms^{-1}]
$\overline{u}$, $\overline{v}$, $\overline{w}$	Mean wind speeds. [ms^{-1}]
$\overline{u'w'}$	Fluctuation covariance (kinematic shear stress or momentum flux) [m^2s^{-2}]
u_*	Friction velocity [ms^{-1}]
h_c	Height of the plant canopy. [m]
$< >$	Spatial averaging of the term within these brackets.
a	Leaf area density of plant parts with a canopy. [m^2m^{-3}]
f	Coriolis force due to the Earth's rotation. ($f = 2\Omega\sin\phi$) [s^{-1}]
Ω	Rotational speed of the Earth. [rad s^{-1}]
ϕ	Latitude on Earth. [°]
u_g, v_g	Geostrophic wind speeds in the horizontal plane above the PBL. [m s^{-1}]
p	Atmospheric pressure. [N m^{-2}]
g	Gravitational acceleration. [m s^{-2}]
C_d	Drag coefficient caused by plant parts in a canopy. [ ]
β	Empirical used to describe wind speed profile. [ ]
L	Monin-Obukhov length. [m]
L_∞	Finite limiting length scale [m]
L_v	Latent Heat of vaporisation [m^2s^{-2}]

S_U	A kinematic source term in a conservation equation. [m s^{-2}]
S_H	Sensible Heat production [Ks^{-1}]
S_v	Vapour production [kg$m^{-3}s^{-1}$]
Q_H	Mean vertical flux of sensible heat [kgs^{-3}]
Q_E	Mean vertical flux of latent heat [kgs^{-3}]
Q_*	Net radiative flux [kgs^{-3}]
T	Temperature [K]
c_p	Specific heat. [$m^2s^{-2}K^{-1}$]
Q	Heat Radiation. [kg m^2s^{-2}]
ψ	Universal dimensionless function used to define vertical wind profile. [ ]
α	Closure constant associated with form drag dissipation. [ ]
δ	Top of the domain in the planetary boundary layer. [ ]
ε	Mean kinetic energy dissipation rate. [m^2s^{-3}]
λ	Algebraic length scale used to describe turbulence eddy size. [m]
κ	Von Kármán constant. [ ]
μ	Proportionality constant for eddy viscosity in TKE. [ ]
ν	Kinematic viscosity. [m^2s^{-1}]
θ	Mean potential temperature. [K]
θ_o	Reference state for the mean potential temperature. [K]
ρ	Air density. [kg m^{-3}]
ρ_0	Air density at reference level. [kg m^{-3}]
σ	Velocity standard deviation. [ms^{-1}]
τ	The turbulent tangential shearing stress at an interface. [kg $s^{-2}m^{-1}$]
τ_h	Kinematic shear stress [m^2s^{-2}]
$\mathfrak{L}$	Eddy size. [m]
$\mathfrak{I}$	Time scale to describe turbulence. [s]
WS77	Wilson and Shaw, 1977.
W98	Wilson et al., 1998.
W88	Wilson, 1988.
KC99	Katul and Chang, 1999.

1 Introduction

Modelling of planetary boundary layer (PBL) winds has important applications in forestry, agriculture, wind energy production, and other disciplines in which there is exchange of energy, momentum, gas, and airborne particles between ground, plants and the atmosphere. The PBL is the portion of the atmosphere that is highly turbulent, and strongly influenced by the effects of the Earth's surface. The lower (approximately) one-tenth of the PBL is identified as a "surface layer", where over a uniform horizontal surface, variables such as the Reynolds stress and turbulent heat flux are approximately constant, both along the vertical axis, and along the horizontal axes. The focus of the present work is on this surface layer, and in particular, the behaviour of wind within a horizontally uniform plant canopy.

The primary problem in boundary layer modelling is parameterising the effects of turbulence. Significant effort has been put towards developing ways to represent eddy flux terms in the averaged conservation equations of motion and other species (heat, water vapour, carbon dioxide, etc.). The eddy viscosity[1] (or "K-theory") model is one such formulation that assures mathematical simplicity and numerical stability when computations are necessary. However, the formulation of K has to reflect the PBL state, which varies both in space (with height z at least; and in general, with location relative to any irregularity of topography or ground cover and condition) and in time (diurnally, seasonally, and in response to passage of synoptic systems). Much research has been devoted towards formulating functional expressions for K appropriate for all states (i.e. the range of stratification) of the PBL over uniform

[1] Introduced by Prandtl early in the 20th century

terrain and even in "disturbed" flows. Higher order schemes have also been developed to solve the turbulence closure problem, but at the expense of added equations and unknowns to solve.

This study compares the performance of a first-order (K) model introduced by Wilson et al. (1998), and two second-order closures described by Katul and Chang (1999; see literature review in following section). The particular K-closure of interest here is the relation $K \propto \lambda\sqrt{k}$ where K is the eddy viscosity, k is the turbulent kinetic energy (TKE), and λ is a heuristic, spatially varying turbulence length scale. The comparison is performed in the context of steady state, horizontally uniform, non-rotating and neutrally buoyant flow in a plant canopy.

The goal of the work is to establish whether there is, practically, any advantage or meaningful gain in accuracy, when the more complex approach (second-order closure) is taken. Katul and Chang sought to establish which was the better second-order model (of two they compared), but did not question whether a first-order closure might in fact have been equally adequate. In entertaining this question we do not dispute the theoretical superiority of a second-order closure. We merely highlight the ambiguities common to both approaches (e.g. how to establish the drag coefficient) and query whether those ambiguities imply that the superiority of second-order closure is rather inconsequential. So the question is, might a first-order closure model do just as well as a higher-order closure, in practise, for simulating wind flow through a (nominally) uniform forest?

1.1 The Study by Katul and Chang (1999)

Two second-order models, one introduced by Wilson and Shaw (1977; hereafter WS77) and the other by Wilson (1988; hereafter W88), were compared by Katul and Chang (1999; hereafter KC99) against measured winds in the Duke Forest of North Carolina. The motive for the study was to find a "simple" model for turbulent velocity statistics at all levels within a uniform plant canopy. In relation to that motive, least it seem arcane, perhaps it is worthwhile to mention that the mean velocity profile and turbulence statistics in a forest canopy must be known in order to attempt rational scientific treatment of a wealth of interesting and important forest processes, such as aerial spray dispersion, or the spread of pollen or plant pathogens - to say nothing of the fact that these statistical properties of the wind modulate the relationships between observable mean properties of the air stream (e.g. mean temperature, humidity and carbon-dioxide concentration) and the inter-related rates of emission/absorption by the forest (leaf transpiration and photosynthesis), relationships which are of great importance in such fields as agronomy and forestry.

The Duke Forest velocity measurements were made on a 20-m tower, standing in a 14-m high loblolly pine forest, using tri-axial sonic anemometers installed at six levels. Signals from these sensors were processed to give mean velocity $\overline{u}$ (horizontal along-wind direction), turbulent shear stress $\overline{u'w'}$ (w' being the vertical velocity fluctuation), velocity standard deviations σ_u, σ_v, and σ_w, and third-order moments. Scaling of these velocity statistics on the friction velocity (u_*) made it possible to compare the normalised profiles of $\overline{u}$, $\overline{u'w'}$, σ_u, σ_w, turbulent kinetic

energy $k = \frac{(\sigma_u^2 + \sigma_v^2 + \sigma_w^2)}{2}$, and the third-order moments against the corresponding profiles from the wind models. The forest itself was characterised in terms of its mean height (h_c=14 m), and its (strongly height-varying) leaf area density[2] $a(z)$, which was measured at approximately 1 m height intervals to the top of the forest. In addition to those properties, the models required as input a foliage drag coefficient; this was inferred from the wind measurements by a procedure that is outlined later in the thesis.

KC99 concluded that WS77 produced a slightly better mean velocity profile $\overline{u}$ but a worse longitudinal velocity standard deviation profile σ_u, than W88; and that the modelled third moments were inconsistent with measurements. In our view these results are of uncertain significance, for as we will later show, a first-order closure model produces mean wind and shear stress profiles every bit as good as (if not better than) those given by KC99 for the second-order models.

In even the simplest second-order closure models of neutrally-stratified turbulence, the conservation equations produce three difficult and unknown terms that require approximations: pressure-strain, momentum flux-transport, and the turbulent kinetic energy dissipation rate. To model these terms requires specification of an empirical characteristic length scale, to be specified as a function of position and of the flow variables. WS77 uses an empirical length scale that varies with height within the canopy. The W88 model proposed a relaxation time scale defined by the ratio of turbulent kinetic energy k to mean kinetic energy dissipation rate ε. According to

[2] The measure of the total leaf surface area per unit volume, centred at a given height

KC99, principal length scales for both models agreed reasonably well with measured integral length scales in the canopy.

1.2 A Puzzle in Katul and Chang (1999)

The KC99 publication contains a contradiction between the values of the normalised[3] TKE $\left(k/u_*^2\right)_{z=h_c}$ plotted on their Figure 1, and the values cited in their Table 3. We have re-plotted their Figure 1 as our Figure 1-1.

By definition, the normalised TKE is

$$\frac{k}{u_*^2} = \frac{(\sigma_u/u_*)^2 + (\sigma_v/u_*)^2 + (\sigma_w/u_*)^2}{2} \qquad \textbf{(1.1)}$$

The measured velocity standard deviations cited by KC99 in their Table 3 are reproduced in Table 1-1 below, and from them we calculated TKE based on Equation (1.1), also shown in Figure 1-1 (fifth column). Our values do not agree with those given by KC99 on their Figure 1. The KC99 simulations of turbulent kinetic energy fitted these (we suspect, **mistaken**) values perfectly.

---

[3] The symbol u_* is friction velocity. It is defined as $u_* = \sqrt{-\overline{u'w'}}$ and is usually prescribed at the top of the model domain or at the top of the plant canopy.

Table 1-1: Calculation of TKE (k) for the Duke Forest from the measured velocity standard deviations cited in KC99 Table 3. The values tabulated for KC99 (final column) were taken from their Figure 1.

z/h_c	σ_u	σ_v	σ_w	$(k/u_*^2)^{Calc}$	$(k/u_*^2)^{KC99}$
1.428	2.51	2.38	1.44	7.02	4.7
1.097	2.08	1.86	1.22	4.64	3.1
0.907	1.91	1.66	1.11	3.82	2.8
0.666	1.25	1.1	0.94	1.83	1.9
0.41	0.55	0.47	0.44	0.36	0.9
0.286	0.57	0.51	0.3	0.34	0.9

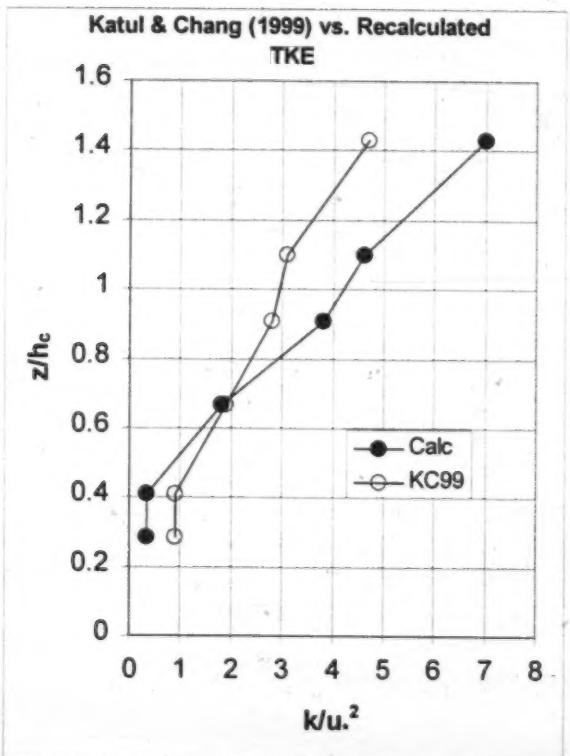

Figure 1-1: Comparing the contradicting values for normalised TKE given by KC99 and the values calculated here from their cited velocity standard deviations. The hollow circles are from Fig. 1 of KC99; the solid circles are our calculated TKE.

1.3 Objectives

The thesis will first review general ideas of the planetary boundary layer (PBL), and the governing equations for turbulent fluid flow. It will then narrow in focus specifically to horizontally-uniform canopy flows. This involves reducing a large set of conservation equations, using several approximations and assumptions, to finally obtain a flow model based on only two conservation equations in two unknowns. These two equations will be discretised, solved numerically, and their solutions compared to measured data from several plant canopies previously studied by Wilson et al. (1998; hereafter W98). Finally, simulations of Duke Forest using the first order model will be compared against the observations and simulations of KC99.

2 The Planetary Boundary Layer

The PBL, sometimes called the "Ekman layer", is a (usually) turbulent layer between the nominally geostrophic outer flow[4], and the solid boundary (earth's surface) at which the no-slip condition applies. The PBL itself is conceived to be sub-dividable into several sub-layers, the most important being the surface layer, the mixed layer, and the entrainment interface layer. These layers are easily demarcated with reference to the idealised (summer, fair-weather) daytime profile of mean potential temperature $\overline{\theta}(z)$, as seen in Figure 2-1 below.

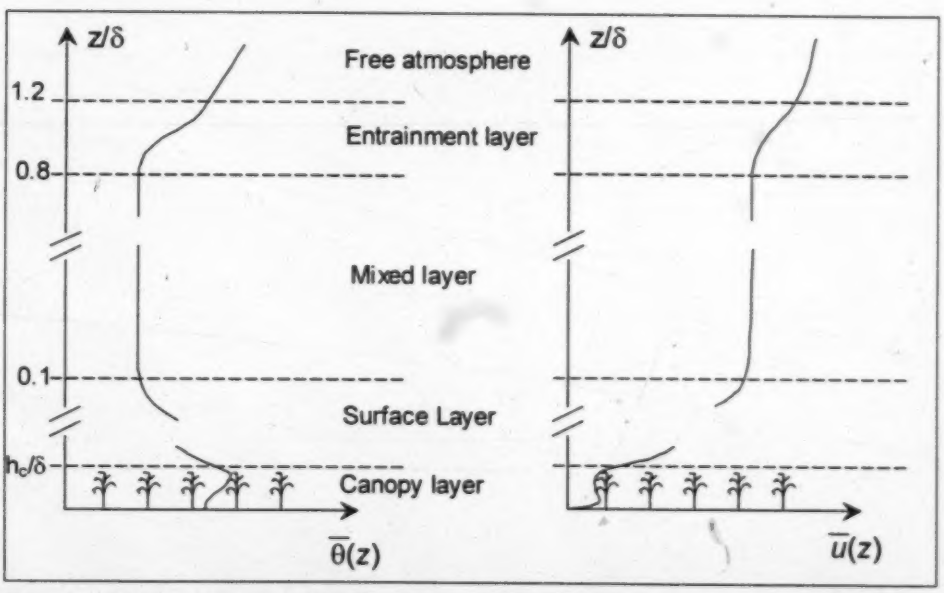

Figure 2-1: Daytime profiles of mean potential temperature and mean horizontal velocity through the PBL, showing basis for conceptual division of the PBL into several sub-layers. The height to the entrainment layer at δ is of the order of 1 km.

[4] The wind is considered geostrophic at the top of the PBL and above. In geostrophic flow the Coriolis force is oriented perpendicular to the direction of flow (to the right in the northern hemisphere and to the left in the southern hemisphere), and exactly balances the pressure gradient (which thus is also perpendicular to the flow). The large-scale horizontal pressure gradients are caused by non-uniform heating and cooling (owing to heating from the sun and radiative cooling out to space above the Earth).

Let us consider a geostrophic free atmosphere, and suppose that there is a uniform horizontal flow with velocity components (u_g, v_g) along axes (x, y) respectively, where x is the positive east direction, and y is the positive north direction (we will alter our co-ordinate system in Section 3). According to the geostrophic equations, associated with u_g there is a pressure (p) gradient in the y direction,

$$fu_g = -\frac{1}{\rho}\frac{\partial p}{\partial y} \tag{2.1}$$

where ρ is air density, and $f = 2\Omega\sin\phi$ is the Coriolis parameter, ϕ being the latitude and Ω the earth's angular velocity ($\Omega = 2\pi / (24\times3600)$ rad/s ; at mid-latitudes $f \sim 10^{-4}$ s^{-1}). Similarly, associated with v_g there is a pressure gradient along x,

$$-fv_g = -\frac{1}{\rho}\frac{\partial p}{\partial x} \tag{2.2}$$

In geostrophic flow, then, the Coriolis and pressure-gradient forces are in balance. But now turning our attention to the turbulent PBL, an extra term enters the force balance, due to the effect of turbulent friction (because of this significant influence of friction in the PBL, this layer also is often called the "friction layer"). From the physical perspective, we can say that the large-scale pressure gradients drive the winds aloft, i.e. supply their momentum, and that the agency of turbulent mixing transfers a part of that momentum across the PBL down to the near-surface flow below, and to the ground (drag on the ground); consequently flow near ground is often considered to be "shear-driven," i.e. the background large-scale pressure

gradient may be considered logically secondary to this "bombarding" momentum flux that drives the near-ground flow.

Mathematically, the momentum balance in the PBL can be described by

$$f\left(\bar{v} - v_g\right) - \frac{1}{\rho}\frac{\partial \tau_{xz}}{\partial z} = 0 \qquad (2.3)$$

$$-f\left(\bar{u} - u_g\right) - \frac{1}{\rho}\frac{\partial \tau_{yz}}{\partial z} = 0 \qquad (2.4)$$

where τ_{xz} and τ_{yz} are the turbulent shear stresses along the x and y axes, respectively, and z is the vertical axis.

The Coriolis force has a dominant influence on the rapid winds aloft, but is conventionally argued (Kaimal and Finnigan, 1994) to be less important in the shallow surface layer, where the frictional forces near the surface reduce the wind speed (and therefore reduce the effect of the Coriolis term). The Coriolis force, and turning of the mean wind, have often been neglected in treatment of the surface layer, even though it has been known for a long time (e.g. Shinn, 1971) that, due to the Coriolis force, the mean wind direction varies greatly with height within deep forest canopies. Thus the Coriolis force should not, really, be neglected.

2.1 Turbulent Momentum Transfer

We need to understand the meaning and origin of the "turbulent shear stresses" τ_{xz} and τ_{yz} that appear in the momentum equations (2.3, 2.4) for the PBL. In that regard, it will help to first consider a (hypothetical) *laminar* flow (see Figure 2-2) near a surface, and to define **viscous** momentum transfer.

When air flows plane-parallel, slipping over adjacent layers, **viscous friction** ensures that the slow-moving layers are encouraged to "come-along faster" (i.e. to accelerate) by the faster-moving layer (above) - while at the same time they (reciprocally) retard the faster-moving layers. That is to say, momentum is passed down the velocity gradient from the fast-moving layer to the slow-moving layer, and this is the process known under the title "Newton's law of viscosity." For the case of a flow of speed $u = u(z)$ moving plane-parallel in direction x parallel to a surface, the flux of momentum (shearing stress) is given by (Newton's Law of viscous friction)

$$\tau_{xz} = -\rho \upsilon \frac{\partial u}{\partial z} \qquad (2.5)$$

where υ is the kinematic viscosity (in effect, defined by this equation), ρ as earlier is the air density, and τ_{xz} is the tangential (shearing) force per unit area of the interface.

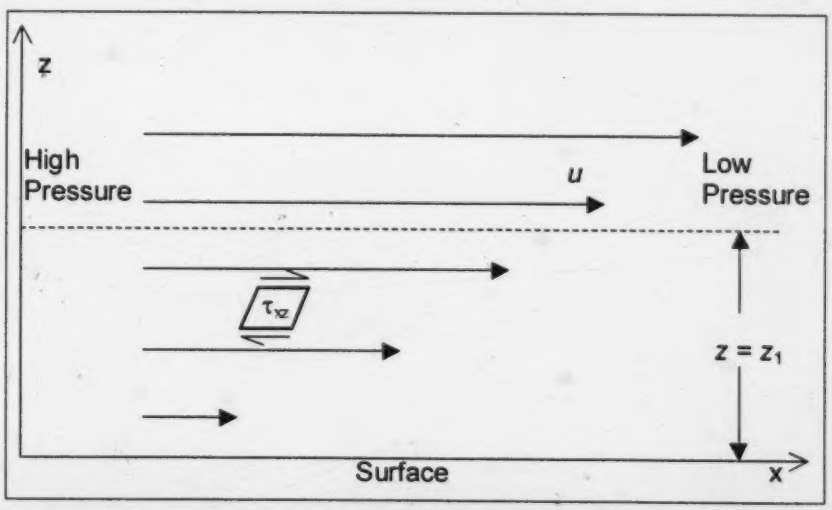

Figure 2-2: A hypothetical laminar flow. The wind speed gradient from top to bottom results in a shear stress according to Equation (2.5)

Now, by definition, in ***turbulent*** flow, cross-stream convective exchanges occur. Air parcels from fast-moving layers descend (are pushed down) into slower moving layers where they "give up" their "excess momentum" to the tardy flow - and vice versa (see Figure 2-3). This bulk-exchange process dramatically increases the rate of cross-stream momentum exchange (mean momentum flux) for a given strength of the (mean) velocity gradient.

Over flat horizontal terrain, we can consider cross-stream momentum exchange as being the consequence of fluctuating vertical motion (w'), and this momentum exchange can be quantified by way of the velocity covariance $\overline{u'w'}$. This covariance, which is derived in Section 3.3, is also called the kinematic shear stress or the momentum flux across the x-z plane i.e. $\tau_{xz} = -\rho\,\overline{u'w'}$. Here we are now making the assumption that the x-direction is aligned with the local wind flow (the longitudinal or along-wind component, u), and that the lateral wind speed $v = 0$. This co-ordinate system is more firmly established in Section 3.

Turbulence dissipates kinetic energy (as heat), and unless a source of energy constantly sustains turbulent motion, turbulence cannot continue to exist. The conditions sustaining turbulence (rapid vertical mixing) are a spatial gradient in average wind speed, known as wind shear (the most important component is usually the vertical shear, $\partial\overline{u}/\partial z$), and unstable buoyancy forces[5] (i.e. warm air from ground heat underlying cold air). The energy balance of turbulence can be analysed precisely by means of a budget equation derived from Navier-Stokes equations (Section 3.3).

[5] In this study we mainly deal with neutrally stratified flow, where buoyancy forces are by definition negligible. However the no-slip condition at the surface requires the velocity there to vanish, resulting in strong wind shear immediately above the surface, and thus strong vertical mixing (turbulence).

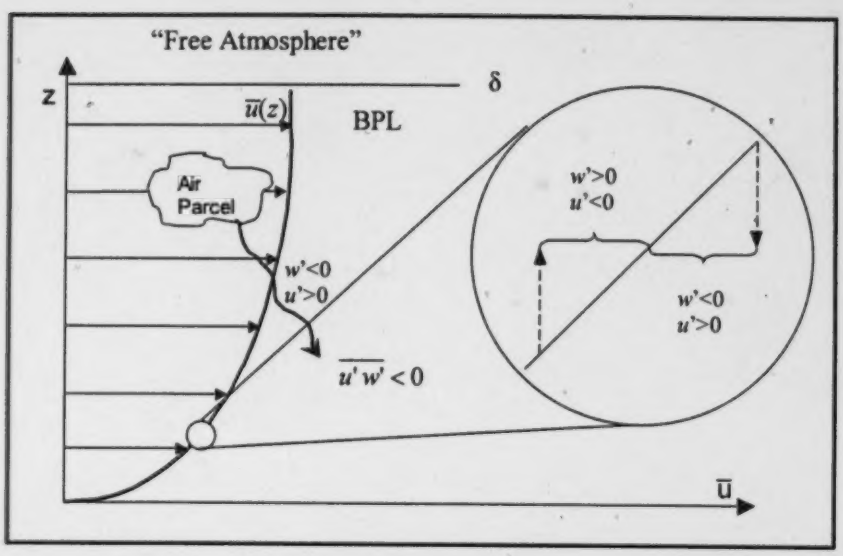

Figure 2-3: Fluctuations u' and w' in horizontal and vertical velocity due to turbulent movement of an air parcel from one level to the next. The velocity covariance $\overline{u'w'}$ represents a kinematic momentum flux; i.e. it quantifies the strength of the turbulent momentum flux due to air parcels moving across horizontal layers in the turbulent flow.

2.2 Characterising Turbulence

"Turbulence" has many quantifiable attributes, and we shall mention only those in common use as "descriptors" of the flow. Perhaps the most important parameters are the standard deviations of the three components of wind velocity, i.e. the root mean square fluctuations:

$$\sigma_i = \sqrt{\overline{u_i'^2}} \text{ or } \sigma_u = \sqrt{\overline{u'^2}}, \sigma_v = \sqrt{\overline{v'^2}}, \sigma_w = \sqrt{\overline{w'^2}}$$

A related parameter is the turbulent kinetic energy (per unit mass, known as "TKE"), defined by

$$k = \frac{1}{2}\left(\sigma_u^2 + \sigma_v^2 + \sigma_w^2\right)$$
$$= \frac{1}{2}\left(\overline{u'u'} + \overline{v'v'} + \overline{w'w'}\right)$$

The velocity standard deviations and the TKE are relatively independent of height in the lower PBL, except in a thin layer[6] immediately against the surface, across that they drop to zero.

The turbulent fluctuations have another "aspect", the duration of eddies, and this is usually characterised by a time scale ($\mathfrak{I}$), which (in a qualitative way) is a typical elapsed time between reversals of the sign of the vertical velocity (a formal definition can be given). The time scale also increases away from the surface. This implies that the "eddy size" $\mathfrak{L} = \mathfrak{I}\sigma_w$ of the turbulent fluctuations in general increases with increasing distance away from the ground. The "eddy size" in the vertical is closely related to the efficiency of the vertical exchange process, that is, it exerts a strong influence on the "exchange coefficient" K (see Section 4.1). This latter term is also known as the "eddy diffusivity" and can usually be approximated as $K \propto z$ near ground.

2.3 The Atmospheric Surface Layer

As indicated earlier, very near the earth's surface is an "inner layer" of the PBL, a layer of particular significance in that it is within this layer that we live, and that most of our daily activities take place. This is the atmospheric surface layer (ASL), and its height is (nominally) 10% of the PBL.

[6] E.g. a forest or crop canopy.

The wind cannot flow through the ground and so in the ASL the average vertical velocity $\overline{w}$ is tiny compared to the average horizontal velocity $\overline{u}$; indeed, $\overline{w}$ is essentially zero over a uniform, horizontal surface. The *mean* flow is parallel to the surface. However, there remains the *fluctuating* vertical velocity (w'; see Section 3.3), and the turbulent eddies are the sole agent for vertical exchange across the ASL.

In the ASL, eddy size is relatively small, because the solid ground prevents organised upward or downward movement on large spatial scale. But vast amounts of heat, water and particulate matter nevertheless are able to travel through the ASL to the outer PBL. This net convective movement is due to the frequent existence of large mean vertical gradients in temperature, humidity, particle concentration, and wind speed (thus, near ground, *small* eddies act on a *large* mean gradient). These strong mean gradients *diminish* with increasing height, hand in hand with *increasing* eddy size (thus an *increasing* exchange coefficient), and in the PBL, above the ASL, the mean gradients become very small (e.g. Figure 2-1). With this idea in mind we can regard the outer PBL as a large and well mixed reservoir of heat, humidity and air borne particles, and the ASL as the "valve" separating that reservoir from the plant canopy and the ground surface.

2.3.1 General Wind Profile in the surface layer of the PBL

In general when studying microscale, steady-state wind flow within the PBL, we focus on *differences* of the flow relative to a "reference flow" or "basic state." The reference state ordinarily is a wind flow over an infinite flat plain, thus, the reference

flow is "horizontally homogenous," and we may say that the reference state is "one-dimensional", meaning that statistical properties vary only on the vertical (z) axis.

The most basic attribute of the "reference flow" will be its profile of mean wind speed, which we represent symbolically as $\overline{u}_0(z)$. Since the flow is slowed down by the drag exerted near the ground (and $\overline{u}_0(z) \rightarrow 0$ as $z \rightarrow 0$, the "no slip condition"), the scale of the surface irregularity (z_o, the surface roughness length) plays a role in defining the shape of the wind profile, which is observed to be logarithmic (in the height z) for a deep, ground-based layer of the neutrally stratified PBL. Allowing for stratification, the vertical wind speed profile within the "constant stress layer" (i.e. surface layer) can be represented by

$$\overline{u}_0(z) = \left(\frac{u_*}{\kappa}\right)\left[\ln\left(\frac{z}{z_o}\right) - \psi\left(\frac{z}{L}\right) + \psi\left(\frac{z_0}{L}\right)\right] \qquad \textbf{(2.6)}$$

where the friction velocity u_* is related to the surface stress τ through the definition $|\tau| = \rho u_*^2$ (ρ is the air density). The von Kármán constant κ is usually taken as 0.40 (Justus, 1978). The parameter L is called the Monin-Obukhov length, z_0 is a surface roughness length, and ψ is a universal dimensionless function (Paulson, 1970) which depends on the atmospheric stability (z/L).

2.3.2 Wind Flow in a Canopy

The surface-layer wind profile (Equation 2.6) is valid only provided the height $z \gg z_o$. However, in the case of a full plant canopy of height h_c, the roughness length $z_o \sim h_c/10$ and so equation (2.6) fails to describe the wind both *in* the canopy, and over

a considerable range in height *above* the canopy. There is no universal wind profile analogous to Equation (2.6) that covers the within-canopy flow, unless we attribute that distinction to the popular empirical profile

$$\overline{u}(z) = \overline{u}(h_c) e^{\beta\left(\frac{z}{h_c} - 1\right)}, \quad z \le h_c \tag{2.7}$$

which is widely adopted for canopy flow (β is an empirical parameter and has the interpretation $\beta = \ln \frac{\overline{u}(h_c)}{\overline{u}(0)}$). The rational approach to describing the mean wind in and above the canopy is to solve the (appropriately simplified) equations of motion – the approach taken here.

As shown in Figure 2-4, the shear stress, TKE and average wind speed vary significantly with height through the canopy layer, and above (these properties stabilise at the top of the PBL at height $z = \delta$, and in fact $k = \overline{u'w'} = 0$ is sometimes taken as the *definition* of the top of the PBL). Near the top ($z = h_c$) of the canopy, there is a region of very strong mean wind shear and steep shear stress divergence. Deeper in the canopy the wind speed is low (and may be nearly constant with height). And of course wind speed vanishes in the limit $z \to 0$.

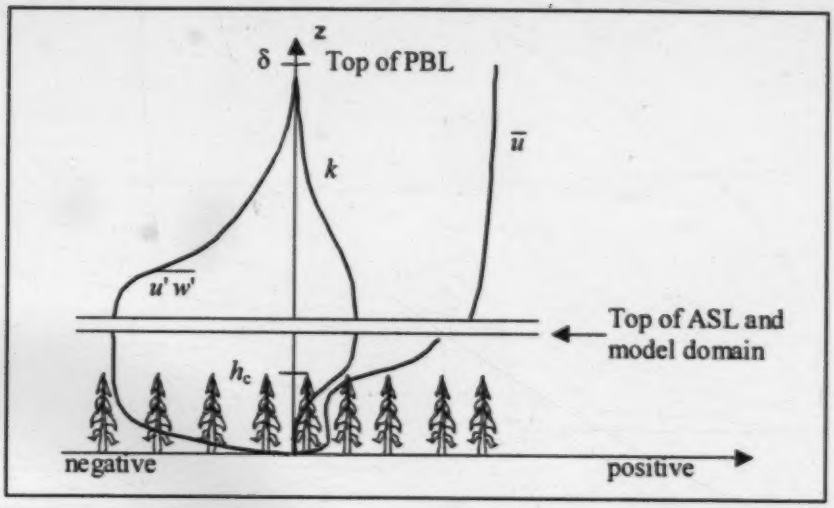

Figure 2-4: Schematic profiles of the principal wind and turbulence statistics, in and above a plant canopy. The height $z = \delta$ represents the top of the PBL. The shear stress divergence ($\partial\overline{u'w'}/\partial z$) within the canopy is balanced by drag on the vegetation (Section 3.4.2, Equation 3.17). Although $\overline{u'w'}$ and k converge to zero at the top of the PBL, they reach a maximum in magnitude at the top boundary of the surface layer as will be seen in Section 5.3.1.

3 Governing Equations

The following sections introduce the conservation equations governing turbulent flow, in rather complete form, then reduce them to the specialised case of interest.

3.1 Co-ordinate System

The system in question is homogenous in both the crosswind (y) and the along-wind (x) directions, but its statistical properties vary with height (z). We choose a co-ordinate system (Figure 3-1) oriented such that the x-axis is aligned with the mean flow, the y-axis is perpendicular and lateral to the mean flow, and the z-axis is vertical.

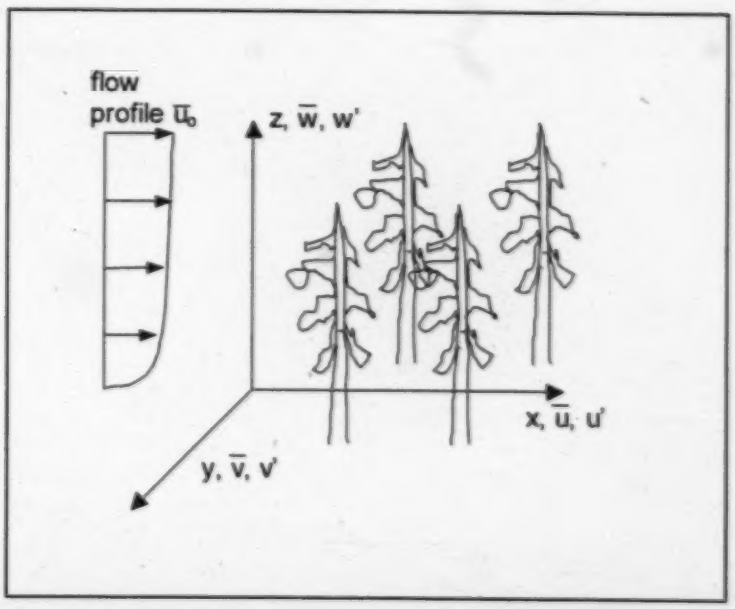

Figure 3-1: Co-ordinate system in a canopy flow. The wind speed $\overline{u}_0$ is the average undisturbed oncoming profile, and $\overline{u}$ and u' are the average and the deviation of wind speed within the canopy. Their sum is the instantaneous wind speed u, i.e. $u = \overline{u} + u'$. The same terminology applies for the lateral and vertical wind speeds v, w.

3.2 Conservation Equations under Boussinesq Approximation

Within the PBL a set of governing equations need to be derived that account for the effects of turbulence. The most important equations for fluid flow are those for conservation of mass, momentum, turbulent kinetic energy and heat (of course, too, the ideal gas law applies). These could be derived in their full form and complexity, but that is unnecessary when attention is restricted to the (rather shallow) PBL.

The basic state density in the lowest kilometre of the atmosphere (PBL) varies by only about 10%, and the density fluctuation (at any level z) is only a few percent of the mean density at z. The Boussinesq approximation assumes that the variations in the density affect the buoyancy term, but may be neglected in the inertial terms of the momentum equations. For the small amplitudes of vertical displacements that are expected in canopy flows, the Boussinesq approximation is always valid (Kaimal and Finnigan, 1994).

3.2.1 Conservation of Mass

The rigorous statement of conservation of mass is

$$\frac{\partial \rho}{\partial t} + \frac{\partial \rho u}{\partial x} + \frac{\partial \rho v}{\partial y} + \frac{\partial \rho w}{\partial z} = 0 \qquad (3.1)$$

where ρ is the air density and u, v, and w are the wind speed in the Cartesian system defined by x, y, and z.

Under the Boussinesq approximation the continuity equation simplifies to a statement that the velocity field is non-divergent,

$$\nabla \cdot \vec{u} = \operatorname{div} \vec{u} = \frac{\partial u_i}{\partial x_i} = \frac{\partial u}{\partial x} + \frac{\partial v}{\partial y} + \frac{\partial w}{\partial z} = 0 \qquad (3.2)$$

The symbol u_i represents the vector velocity, i.e. $u_i = (u_1, u_2, u_3) = (u, v, w)$. The grad operator ∇ is shorthand for $\partial / \partial x_i$ [7].

3.2.2 Conservation of Momentum

The equations of motion (in advection form) under the Boussinesq approximation are

$$\frac{Du}{Dt} = \frac{\partial u}{\partial t} + u\frac{\partial u}{\partial x} + v\frac{\partial u}{\partial y} + w\frac{\partial u}{\partial z} = -\frac{1}{\rho_0}\frac{\partial p}{\partial x} + fv + \nu\nabla^2 u \qquad (3.3)$$

$$\frac{Dv}{Dt} = \frac{\partial v}{\partial t} + u\frac{\partial v}{\partial x} + v\frac{\partial v}{\partial y} + w\frac{\partial v}{\partial z} = -\frac{1}{\rho_0}\frac{\partial p}{\partial y} - fu + \nu\nabla^2 v \qquad (3.4)$$

$$\frac{Dw}{Dt} = \frac{\partial w}{\partial t} + u\frac{\partial w}{\partial x} + v\frac{\partial w}{\partial y} + w\frac{\partial w}{\partial z} = -\frac{1}{\rho_0}\frac{\partial p}{\partial z} + g\frac{\theta}{\theta_0} + \nu\nabla^2 w \qquad (3.5)$$

Here ρ_0 is a constant mean value for density. Other variables are the pressure departure p from a hydrostatic reference state, the Coriolis parameter f, the gravitational acceleration g, and the departure θ of potential temperature from its

---

[7] For an atmospheric layer or motion that is much deeper that the PBL, such as a cumulonimbus cloud, the Boussinesq approximation is unrealistic. Mean density gradients are non-negligible, and essential for properly representing buoyancy force. Thus we have a relation known as the deep convection continuity equation (Pielke, 1984)

$$\frac{\partial}{\partial x_j}(\rho_0 u_j) = 0$$

This more complex statement of mass conservation is necessary if the vertical depth of circulation is on the same order as the density scale depth. The parameter $\rho_0 = \rho_0(x, y, z)$ is defined as a synoptic scale reference, or temporally constant mean, density. Most often ρ_0 is regarded as varying only in the vertical, $\rho_0 = \rho_0(z)$. This form of the conservation-of-mass relation eliminates sound waves (Pielke, 1984) as a possible solution and can be referred to as the anelastic, or soundproof, assumption.

(constant) basic state value, θ_0. The term $\nu\nabla^2\bar{u}$ is the viscous friction, which can usually be neglected.

3.2.3 Conservation of Heat

The thermodynamic energy equation has the form

$$\frac{D\theta}{Dt} = \frac{\partial\theta}{\partial t} + u\frac{\partial\theta}{\partial x} + v\frac{\partial\theta}{\partial y} + w\frac{\partial\theta}{\partial z} = \kappa\nabla^2\theta + S_\theta \qquad (3.6)$$

S_θ represents the sources and sinks of heat including freezing and melting, condensation and evaporation, deposition and sublimation, radiative divergence, etc. The term κ is the molecular thermal diffusivity, and $\kappa\nabla^2\theta$ is the divergence of the molecular heat flux.

Because molecular transfer of heat (through diffusion) or other properties of the air is very slow relative to exchange by the bulk (convective) motion of fluid, we may usually set the right hand side to zero.

3.3 Reduction of Conservation Equations to Reynolds Equations

3.3.1 Time Averaging

The atmosphere is a continuum, in motion on a vast range of length scales. We will never have (nor even wish to have) knowledge of the state of motion at every point, at every instant. So it becomes necessary to define what are to be the "resolved" and "unresolved" scales of motion, and to approximate the influence of the unresolved scales on the resolved. For example, let us consider the velocity component u_i. It can be decomposed into the sum of the average $\overline{u}_i$ and the deviation

from the average u_i', i.e. $u_i = \overline{u}_i + u_i'$. The average is the resolved component and the deviation (also known as the "fluctuation") is the unresolved component.

The unresolved field plays an important role in the evolution of the average; i.e. it may act so as to change the average over time. Parameterisation of that influence is the role of a "closure model" (see Section 4), which is formulated in terms of statistics of the fluctuations u_i', θ', etc. In the first order closure, the influence of the unresolved turbulent eddies is treated as equivalent to an increased viscosity of the fluid. In contrast, a higher order closure consists of a set of differential equations for statistics of the unresolved motion, these being derived from the Navier-Stokes equations.

3.3.2 Applying Averaging to Conservation Equations

The averaged form of the conservation equations is obtained by substituting $u_i = \overline{u}_i + u_i'$ (etc.) and averaging. The resulting equations are known as the Reynolds Equations:

$$\frac{\partial \overline{u}_i}{\partial x_i} = \frac{\partial \overline{u}}{\partial x} + \frac{\partial \overline{v}}{\partial y} + \frac{\partial \overline{w}}{\partial z} = 0 \qquad \textbf{(3.7)}$$

$$\frac{\partial \overline{u}}{\partial t} + \overline{u}\frac{\partial \overline{u}}{\partial x} + \overline{v}\frac{\partial \overline{u}}{\partial y} + \overline{w}\frac{\partial \overline{u}}{\partial z} = -\frac{1}{\rho_0}\frac{\partial \overline{p}}{\partial x} + f\,\overline{v} - \left[\frac{\partial \overline{u'u'}}{\partial x} + \frac{\partial \overline{u'v'}}{\partial y} + \frac{\partial \overline{u'w'}}{\partial z}\right] \qquad \textbf{(3.8)}$$

$$\frac{\partial \overline{v}}{\partial t} + \overline{u}\frac{\partial \overline{v}}{\partial x} + \overline{v}\frac{\partial \overline{v}}{\partial y} + \overline{w}\frac{\partial \overline{v}}{\partial z} = -\frac{1}{\rho_0}\frac{\partial \overline{p}}{\partial y} - f\,\overline{u} - \left[\frac{\partial \overline{v'u'}}{\partial x} + \frac{\partial \overline{v'v'}}{\partial y} + \frac{\partial \overline{v'w'}}{\partial z}\right] \qquad \textbf{(3.9)}$$

$$\frac{\partial \overline{w}}{\partial t} + \overline{u}\frac{\partial \overline{w}}{\partial x} + \overline{v}\frac{\partial \overline{w}}{\partial y} + \overline{w}\frac{\partial \overline{w}}{\partial z} = -\frac{1}{\rho_0}\frac{\partial \overline{p}}{\partial z} + g\frac{\overline{\theta}}{\theta_0} - \left[\frac{\partial \overline{w'u'}}{\partial x} + \frac{\partial \overline{w'v'}}{\partial y} + \frac{\partial \overline{w'w'}}{\partial z}\right] \qquad \textbf{(3.10)}$$

$$\frac{\partial \overline{\theta}}{\partial t} + \overline{u}\frac{\partial \overline{\theta}}{\partial x} + \overline{v}\frac{\partial \overline{\theta}}{\partial y} + \overline{w}\frac{\partial \overline{\theta}}{\partial z} = -\overline{w}\frac{\partial \theta_0}{\partial z} - \left[\frac{\partial \overline{\theta' u'}}{\partial x} + \frac{\partial \overline{\theta' v'}}{\partial y} + \frac{\partial \overline{\theta' w'}}{\partial z}\right] \qquad \textbf{(3.11)}$$

The terms in the square brackets represent the influence of the unresolved scales on the resolved flow ($\overline{u}_i$, $\overline{\theta}$), and mathematically have the form of spatial gradients of various turbulence co-variances. For example, $R_{ij} = \overline{u_i' u_j'}$ is the Reynolds stress tensor (shear stress, momentum flux) and its divergence $\partial R_{ij} / \partial x_j$ is the "turbulent friction" in the $\overline{u}_i$ - momentum equation.

The effects of the unresolved scales, i.e. the unknown terms in brackets, need to be accounted for by some approximation (a "turbulence closure scheme").

3.3.3 Turbulent Kinetic Energy

By means of a tedious algebraic manipulation through averaging of the Navier-Stokes equations (3.3 to 3.5) one may derive individual conservation equations for the three velocity variances $\overline{u'^2}, \overline{v'^2}, \overline{w'^2}$ and (by addition) for (half) their sum, $k = \frac{1}{2}\left(\overline{u'^2} + \overline{v'^2} + \overline{w'^2}\right)$.

Symbolically, the $\overline{u'^2}, \overline{w'^2}$ equations look like[8]:

$$\frac{\partial \overline{u'^2}}{\partial t} + \vec{\overline{u}} \cdot \nabla \overline{u'^2} = -2\overline{u' w'}\frac{\partial \overline{u}}{\partial z} + \ldots - \varepsilon_u \qquad \textbf{(3.12)}$$

$$\frac{\partial \overline{w'^2}}{\partial t} + \vec{\overline{u}} \cdot \nabla \overline{w'^2} = -2\frac{g}{T_0}\overline{w' T'} + \ldots - \varepsilon_w \qquad \textbf{(3.13)}$$

[8] Given later in more detail as Equation (4.7).

Many terms have not been shown, and these equations have been given only to show the origin of the key production terms (shear production, buoyant production) in the TKE budget given in full below.

By summation, the conservation equation for the TKE is

$$\frac{\partial \bar{k}}{\partial t} + \bar{u}\frac{\partial \bar{k}}{\partial x} + \bar{v}\frac{\partial \bar{k}}{\partial y} + \bar{w}\frac{\partial \bar{k}}{\partial z} = -\overline{u'w'}\frac{\partial \bar{u}}{\partial z} + \frac{g}{T_0}\overline{w'T'} + PT_t - \varepsilon \qquad \textbf{(3.14)}$$

The first term on the right is the shear production; it is normally positive, i.e. a source of TKE. The second term is buoyant production, and may either be a source (if the kinematic heat flux density $\overline{w'T'}$ is positive, i.e. in unstable stratification), or a sink in stable stratification. The 3rd and 4th terms are shown only symbolically; the 3rd term is (pressure + turbulent) transport, and is usually parameterised mathematically in flow *models* as the *diffusion* of TKE. The 4th term is the viscous dissipation (the rate at which turbulent kinetic energy is converted into heat by doing work against viscous stress) and it is further described in Section 4.1.2.

3.4 Applying the Reynolds Equations to Canopy Flow

3.4.1 Specialisation to Canopy Flow

The canopy flow in question is assumed be *horizontally homogenous, steady state, unaffected by Coriolis, and neutrally stratified.*

In micrometeorology, "horizontally homogenous" means the statistical properties do not change in the horizontal directions. A host of terms vanish from Equations (3.8 – 3.11) under that restriction.

The restriction "steady state" implies that velocity statistics do not change with time. This means the local tendency terms ($\partial/\partial t$) in Equations (3.8 – 3.11) are negligible.

In the surface layer, if we neglect any wind turning with height, me may align the co-ordinate system so that $\overline{v} = 0$. It has been shown however (Shinn, 1971) that the Coriolis effect does affect flows within a canopy and is not small compared to frictional drag forces. This is not addressed in this study but should be in the future.

The restriction to "neutral stratification" implies that we exclude conditions where buoyancy effects are important. Generally, stability effects are regarded as vanishing in the limit $z/|L| \to 0$, but this may be untrue in a plant canopy. However, provided the wind speed is moderate to strong, our neglect of the influence of stratification should be unimportant. Under these restrictions, the $\overline{u}$ -momentum equation reduces to

$$0 = -\frac{1}{\rho_0}\frac{\partial \overline{p}}{\partial x} - \frac{\partial \overline{u'w'}}{\partial z} \qquad \textbf{(3.8')}$$

3.4.2 Need for Spatial Averaging

At this point we must clarify, what does "horizontally homogenous" mean in a plant canopy? In general the mean velocity $\overline{u}$ in the airspace between plants is non-zero. But what is the value of $\overline{u}$ "on" or "at" a plant? Zero, presumably. What is the value of $\overline{u}$ in a plant part? It is undefined.

The air within a plant canopy defines a "multiply-connected space" around the plant parts, and the plants are of course excluded from that space. It is only reasonable to speak of horizontal uniformity of properties that have been horizontally averaged over an area that is large with respect to the scale of interplant spacing. Therefore, spatial averaging is logically essential (Wilson and Shaw, 1977; Raupach and Shaw, 1982), and we shall temporarily signify it by angle brackets, < >. Thus $<\overline{u}>$ is the area-averaged mean velocity, defined at all points on, and constant on, horizontal planes, and $\overline{u}_i = <\overline{u}_i> + \overline{u}_i''$.

When this horizontal averaging is carefully applied to the governing equations, the interesting result is that new source terms appear in the thus-averaged equations (Wilson and Shaw, 1977). For example, the $<\overline{u}>$ momentum equation in horizontally uniform flow is not Equation (3.8′) but

$$\frac{\partial <\overline{u}>}{\partial t} = 0 = -\frac{\partial}{\partial z}\left[<\overline{u'w'}> + <\overline{u}''\overline{w}''>\right] - \frac{1}{\rho_0}\frac{\partial \overline{p}}{\partial x} + S_U \qquad \textbf{(3.15)}$$

There are two new terms relative to Equation (3.8′). The "dispersive flux" $<\overline{u}''\overline{w}''>$ is the spatial correlation of local departures of mean velocity from the spatial mean, i.e. $\overline{u}'' \equiv \overline{u} - <\overline{u}>$. This is impossible to measure and can only be

modelled by a fully three-dimensional flow description. It is believed to be negligible – perhaps a concession to feasibility.

The more important new term is S_U, which upon detailed inspection is the net viscous and form drag (in the x-direction) on plant parts. It has to be parameterised, and conventionally it is modelled in terms of the resolved velocity as

$$S_U = -C_d(z)a(z)\overline{u}\sqrt{\overline{u}^2 + \overline{v}^2 + \overline{w}^2} \qquad \textbf{(3.16)}$$

where C_d is the effective drag coefficient of the plants and $a(z)$ is the leaf area density (plant surface area per unit volume) of the plants. We have dropped the < > notation (it is henceforth implied). Because $\overline{w} \approx 0$ (horizontal surface) and $\overline{v} = 0$ by choice of co-ordinates, we shall simplify (3.16) to $S_U = -C_d a\overline{u}|\overline{u}| = -C_d a\overline{u}^2$, because in the flows of interest there is no reason to expect flow reversal (favourable or zero pressure gradient; uniform flow resistance).

Under the conditions described above many of the terms in the averaged conservation equations derived under the Boussinesq approximation have become negligible. The Reynolds equations have produced one single remaining equation, in which the airflow within the canopy is controlled by a balance between the divergence of the streamwise momentum flux, and the drag of the plant parts. This balance is the time average momentum equation, obtained by substituting (3.16) into (3.15),

$$\frac{\partial \overline{u'w'}}{\partial z} = -C_d a(z)\overline{u}^2 - \frac{1}{\rho_0}\frac{\partial \overline{p}}{\partial x} \qquad \textbf{(3.17)}$$

The horizontal pressure gradient is generally non-zero in wind tunnel flows but often negligible in free atmosphere flows. A discussion on modelling the shear stress $\overline{u'w'}$ follows in section 4.

3.4.3 Other Equations for the Horizontally Uniform Plant Canopy

Under the restrictions listed above, the TKE equation can be reduced to

$$\frac{\partial k}{\partial t} = 0 = -\overline{u'w'}\frac{\partial \overline{u}}{\partial z} + \frac{g}{T_0}\overline{w'T'} + PT_t - \varepsilon \qquad \textbf{(3.18)}$$

The mean temperature equation reduces to

$$\frac{\partial \overline{\theta}}{\partial t} = 0 = -\frac{\partial}{\partial z}\overline{w'T'} + S_H \qquad \textbf{(3.19a)}$$

where S_H is of origin similar S_U, and represents the total production of sensible heat due to sources (heat shed by or absorbed by plant material). Similarly, conservation of vapour is expressed by

$$\frac{\partial \overline{\rho}_v}{\partial t} = 0 = -\frac{\partial}{\partial z}\overline{w'\rho_v'} + S_V \qquad \textbf{(3.19b)}$$

where ρ_v is the absolute humidity, and S_V is the vapour production (transpiration or evaporation from wet leaves) or absorption (deposition of dew on plant parts) by plant surfaces. Finally, an overall energy constraint applies:

$$\frac{\partial}{\partial z}\left(\rho c_p \overline{w'T'} + L_v \overline{w'\rho_v'}\right) = \frac{\partial Q_*}{\partial z} \qquad \textbf{(3.20)}$$

where c_p is the specific heat of the air, L_v is the latent heat of vaporisation, Q^* is the net radiation[9], and $Q_H = \rho c_p \overline{w'T'}$, $Q_E = L_v \overline{w'\rho_v'}$ are the mean vertical fluxes of sensible and latent heat.

3.5 Drag Coefficient

Equation (3.16) defines a local drag coefficient (that appears in our momentum Equation 3.17) parameterising the surface area of the leaves and limbs of a plant canopy. The drag coefficient exerts a controlling influence on the aerodynamic properties of the wind amongst the plants, so that its specification is very important. A key aim of this thesis is to indicate that, in practise, it is impossible to determine C_d with a high degree of precision, and in consequence uncertainty in C_d may render pointless any debate as to the superiority of one model over another. We shall illustrate this point in the following section by reference specifically to observations made by KC99 in the Duke Forest (Section 1.1).

The drag coefficient can be defined at three levels of detail, based on the depth and quality of our knowledge of the leaf area density, and of the flow variables $\overline{u}$, and $\overline{u'w'}$. These three levels are as follows:

3.5.1 Height Variable Drag Coefficient

Theoretically the most comprehensive way to calculate the drag coefficient from given micrometeorological measurements would be to calculate $C_d(z)$ by rearranging Equation (3.17),

[9] Here we have neglected photosynthesis and other small terms such as heat capacity of the plants.

$$C_d(z) = \frac{-\frac{\partial \overline{u'w'}}{\partial z} - \frac{1}{\rho_0}\frac{\partial \overline{p}}{\partial x}}{a(z)\overline{u}^2(z)} \qquad (3.21)$$

although evidently this formula will be troublesome (noisy) anywhere that $\overline{u}$ or a become small. If we neglect the pressure gradient, which is acceptable for full scale flows, and normalise the height z with the canopy height h and the velocity components with u_*, we can transform the above to

$$C_d(z) = \frac{-\frac{\partial}{\partial z/h}\left(\overline{u'w'}/u_*^2\right)}{ha(z)\left(\overline{u}(z)/u_*\right)^2} = \frac{-\Delta\left(\overline{u'w'}/u_*^2\right)}{\Delta\left(\frac{z}{h}\right)h\,a(z)\left(\overline{u}(z)/u_*\right)^2} \qquad (3.22)$$

In Equation (3.20) the Δ operator implies a "finite difference" along the height axis, and it is evident that given such finite differences we may calculate $C_d(z)$.

In the Duke Forest of KC99 mean wind and shear stress were measured at six points in and above the canopy. The data for $\overline{u}$ velocity, kinematic shear stress $\overline{u'w'}$, and the leaf area density a are plotted in Table 3-1 along with two different estimates of the drag coefficient.

By one method of estimation, the coefficient C_d (shown as $C_d(z)$ in Table 3-1) is calculated using Equation (3.22) and the five levels within the canopy using measured data for $\overline{u}/u_*$, $\overline{u'w'}/u_*^2$, and $a(z)$. For example, to evaluate the finite difference in the normalised shear stress $\overline{u'w'}/u_*^2$ at a height of 9.32 m, the values for $\overline{u'w'}/u_*^2$ are taken at one level above (at 12.7 m) and at one level below (at 5.74 m), and their difference is divided by the height difference between those two levels.

Table 3-1: Measured mean winds, shear stress, and leaf area density in the Duke Forest of KC99. The drag coefficients C_d and C_{dp} have been calculated based on the given Duke Forest data, using Equation (3.23, 3.24). The five numbers in italics in the $a(z)$ column are interpolated data. Note that the (calculated) drag coefficient becomes negative at the bottom of the canopy.

z/h	z(m)	$\overline{u}/u_*$	$\overline{u'w'}/u_*^2$	a(z)	$C_d(z)$	$C_{dp}(z)$
1.428	19.99	5.53	-1.19	0		
1.097	15.36	3.82	-1	0		
1	14			0		
	13.1			0.008		0.07
0.907	12.70	3.2	-0.93	*0.009*	0.606	
	12.5			0.01		0.08
	11.5			0.05		0.08
	10.5			0.09		0.10
	9.5			0.37		0.13
0.666	9.32	1.44	-0.65	*0.569*	0.116	
	8.5			1.5		0.17
	7.5			0.34		0.22
	6.5			0.84		0.30
0.41	5.74	0.67	0.02	*0.331*	0.848	
	5.5			0.17		0.41
	4.5			0.11		0.54
0.286	4.00	0.62	0.02	*0.095*	-0.095	
	3.5			0.08		0.66
	2.5			0.04		0.52
	1.5			0.1		-2.38
	0.5			0.08		-119.48
	0	0	0	0		

Typically in experimental data, the values for $\overline{u'w'}/u_*^2$ and $\bar{u}/u_*$ are known poorly at an irregularly spaced set of points. To alleviate this difficulty, each discrete profile can be fitted with a continuous polynomial curve, and the resulting functions can be substituted into Equation (3.22), resulting in the form

$$C_{dp}(z) = \frac{F_r(z_n) - F_r(z_s)}{(z_n - z_s)\, F_a(z_c)\, F_u^{\,2}(z_c)} \qquad (3.23)$$

where z_n and z_s are the neighbours above and below z_c. The functions to substitute in this equation are "best fit" polynomials for each data set for the Duke Forest data, viz.

$$F_u = -0.0009z^4 + 0.0031z^3 - 0.018z^2 + 0.1513z$$

$$F_r = 0.0006z^3 - 0.0189z^2 + 0.069z \qquad (3.24)$$

$$F_a = 0.0004z^3 - 0.0154z^2 + 0.145z$$

These polynomial functions are plotted in Figure 3-2 in comparison with the raw measurements.

The resulting drag coefficient is shown as $C_{dp}(z)$ in Table 3.1 and on Figure 3-4. Negative values of C_{dp} are calculated deep in the canopy, this nonsensical result being due to a positive slope in the shear divergence. That (apparent) stress gradient is probably merely measurement error, for the velocity variances, and therefore the velocities themselves, are very small deep in the canopy, implying great difficulty with accurate $\overline{u'w'}/u_*^2$ measurements.

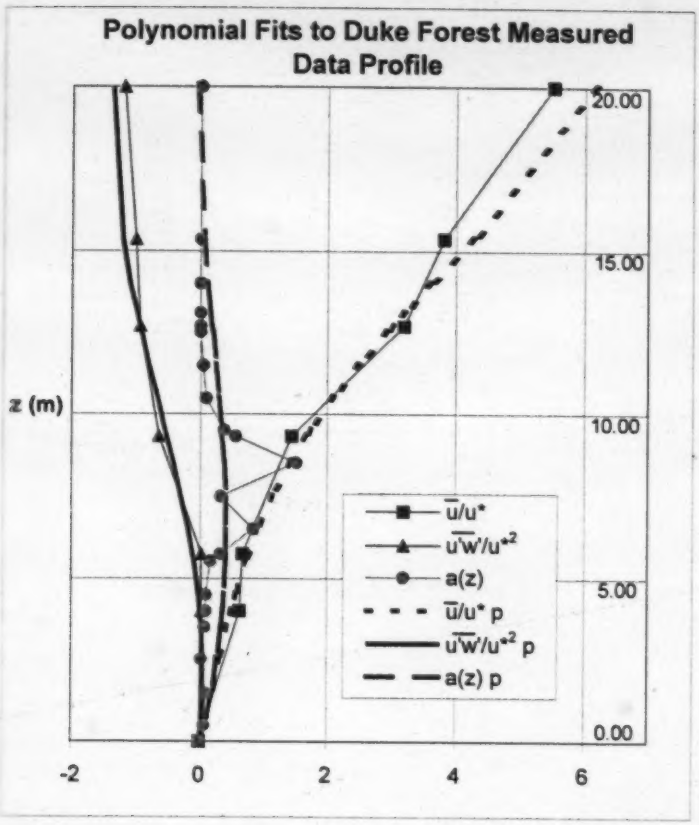

Figure 3-2: Measured values of normalised wind statistics in Duke Forest are fitted with a "best fit" polynomial curve, shown in the legend accompanied with a "p".

Note in Figure 3-2 above that the "best fit" polynomial curve for leaf area density $a(z)$ does not fit very well to the measured values. Thus, defining a height-variable drag coefficient based solely on polynomials is difficult and ambiguous. Perhaps a combination of polynomials for $\overline{u}$, $\overline{u'w'}$ and interpolated data for $a(z)$ would be desired to make the variable drag coefficient more representative of the canopy.

3.5.2 Height Averaged Drag Coefficient

If we have poor information on $\overline{u'w'}$ but good confidence in *a(z)* and $\overline{u}(z)$ then we can use a height-averaged drag coefficient $\overline{C_d}$ in the appropriate momentum equation

$$\frac{\partial \overline{u'w'}}{\partial z} = -\overline{C_d}\, a(z)\, \overline{u}(z)^2 - \frac{1}{\rho_0}\frac{\partial \overline{p}}{\partial x} \tag{3.25}$$

The averaged drag coefficient $\overline{C_d}$ can be defined by integrating Equation (3.25) (again ignoring pressure gradient) as

$$\int_0^h \frac{\partial \overline{u'w'}}{\partial z}\, dz = -\tau_h + \tau(0) = -\tau_h + 0 = -\overline{C_d} \int_0^h a(z)\, \overline{u}(z)^2\, dz \tag{3.26}$$

where the kinematic stress $\tau_h = -\left(\overline{u'w'}\right)_h$, and we have assumed the stress on the ground vanishes (i.e. dense canopy). Rearranging,

$$\overline{C_d} = \frac{\tau_h}{\int_0^h a(z)\, \overline{u}(z)^2\, dz} = \frac{\tau_h / u_*^2}{\int_0^h a(z) \left(\overline{u}(z) / u_*\right)^2 dz} = \frac{1}{\int_0^h a(z) \left(\overline{u}(z) / u_*\right)^2 dz} \tag{3.27}$$

The drag coefficient $\overline{C_d}$ is calculated using the far right term of Equation (3.27), and is approximated as

$$\overline{C_d} = \frac{1}{\sum_{i=1}^{N} q_i \left(z_{i+1} - z_{i-1}\right)} \tag{3.28a}$$

$$q_i = \tfrac{1}{2}\left(a\left(\frac{\overline{u}}{u_*}\right)^2 \Bigg|_{i-1} + a\left(\frac{\overline{u}}{u_*}\right)^2 \Bigg|_{i+1} \right) \tag{3.28b}$$

where, for the case of the Duke Forest canopy, the sum in the denominator of Equation (3.28a) was calculated at the five lowest measurement levels (N = 1,2,3,4,5).

In Table 3-2 below, the $q_i\Delta z$ column contains numbers that are calculated using Equation (3.28b) and the denominator on the right side of Equation (3.28a).

Table 3-2: Data for derivation of a height-independent drag coefficient for the Duke Forest (h_c = 14 m). (KC99 provide $\overline{u}/u_*$ and $a(z)$) The first three columns are used to calculate the height averaged drag coefficient $\overline{C_d}$ = 0.2. The last column shows the height variable $\overline{C_d}\,ah$ using column $a(z)$ multiplied by $\overline{C_d}$ = 0.2.

z(m)	$\overline{u}/u_*$	$a(z)$	$q_i\Delta z$	$\overline{C_d}\,a(z)h$
19.99	5.53	0		
15.36	3.82	0	0.13	0.00
14		0		0.00
13.1		0.008		0.02
12.70	3.2	0.009	2.15	0.03
12.5		0.01		0.03
11.5		0.05		0.14
10.5		0.09		0.26
9.5		0.37		1.06
9.32	1.44	0.569	2.38	1.63
8.5		1.5		4.29
7.5		0.34		0.97
6.5		0.84		2.40
5.74	0.67	0.331	0.16	0.95
5.5		0.17		0.49
4.5		0.11		0.31
4.00	0.62	0.095	0.07	0.27
3.5		0.08		0.23
2.5		0.04		0.11
1.5		0.1		0.29
0.5		0.08		0.23
0	0	0		0.00
		$\Sigma q_i\Delta z$ =	4.89	
		$\overline{C_d} = 1/\Sigma q_i\Delta z$ =	0.20	

This approach to calculating $\overline{C_d}$ with $a(z)$ and the mean wind speed $\overline{u}(z)$ avoids the differentiation of noisy $\overline{u'w'}$ data. And our independently calculated value, $\overline{C_d}$ =0.2, is the same as the drag coefficient cited by KC99 (whose procedure for deriving the drag coefficient was not documented).

3.5.3 Bulk Drag Coefficient

If we have poor or non-existent information on the leaf area density profile $a(z)$, then we have no choice but to use a bulk coefficient $\overline{C_d a}$, which is defined by

$$\int_0^h \frac{\partial \overline{u'w'}}{\partial z} dz = -\tau_h + 0 = -\overline{C_d a} \int_0^h \overline{u}(z)^2 dz \qquad (3.29)$$

Rearranging,

$$\overline{C_d a} = \frac{u_{*h}^2}{\int_0^h \overline{u}^2 dz} = \frac{1}{\int_0^h \left(\frac{\overline{u}}{u_{*h}}\right)^2 dz} \qquad (3.30)$$

It is convenient to define a dimensionless bulk coefficient $C_{db} = h\overline{C_d a}$, which can be evaluated solely from the normalised wind profile in the canopy as

$$C_{db} = \frac{1}{\int_0^h \left(\overline{u}/u_*\right)^2 d(z/h)} \qquad (3.31)$$

Once known, the bulk drag coefficient may be imposed in a normalised momentum equation, viz.

$$\frac{\partial \overline{u'w'}/u_{*h}^2}{\partial(z/h)} = -C_{db}\left(\frac{\overline{u}}{u_*}\right)^2 - \frac{\partial\left(\overline{p}/\rho_0 u_{*h}^2\right)}{\partial x} \qquad (3.32)$$

Table 3-3 and Figure 3-3 show how C_{db} has here been calculated for Duke Forest (C_{db}=0.34).

Our various estimates of the drag coefficient ($C_d(z)$, $C_{dp}(z)$, that of KC99) are shown in Figure 3-4.

Table 3-3: Measured $\overline{u}/u_*$ profile is used to calculate C_{db} using Equation 3.32.

z/h	$\overline{u}/u_*$	$(\overline{u}/u_*)^2$	$(\overline{u}/u_*)^2\Delta(z/h)$
1	3.50	12.27	1.05
0.91	3.2	10.24	1.48
0.67	1.44	2.07	0.32
0.41	0.67	0.45	0.05
0.29	0.62	0.38	0.05
0	0	0	
		$\Sigma(\overline{u}/u_*)^2\Delta(z/h)=$	2.96
	$C_{db}=$	$1/\Sigma(\overline{u}/u_*)^2\Delta(z/h)=$	0.34

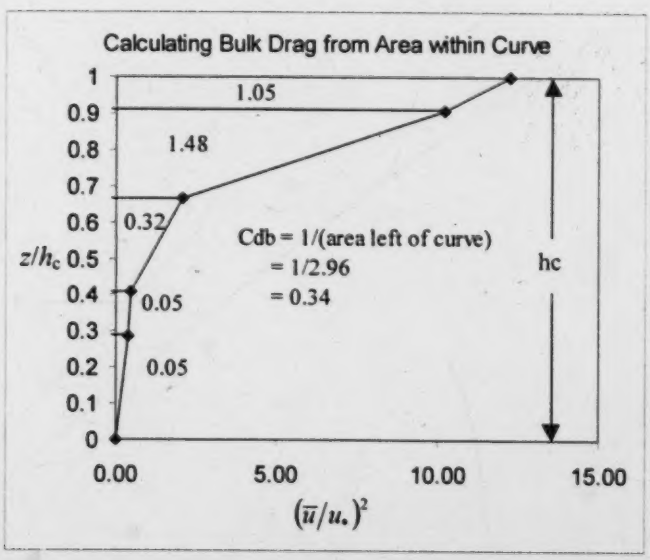

Figure 3-3: As seen here, C_{db} is calculated as the reciprical of the total area to the left of the $(\overline{u}/u_*)^2$ curve.

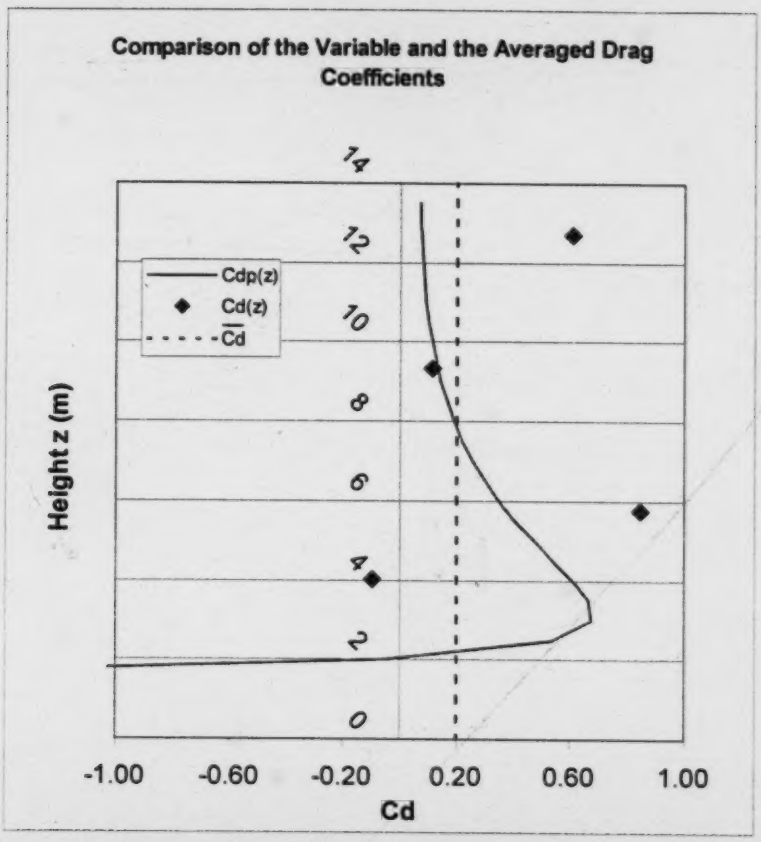

Figure 3-4: The calculated (polynomial-based) drag coefficient $C_{dp}(z)$ is negative at the ground and positive above $z = 2$ m. The plot for (finite-difference based) $C_d(z)$ is highly variable and shows how sensitive it can be to noise in the shear stress gradient. The value for the height-averaged drag coefficient $\overline{C_d}$ (which is the same for both our calculation and that of KC99) is shown for comparison.

4 Turbulence Closures

A "turbulence closure" is an empirical relationship that specifies the influence of unresolved turbulent scales of motion on the modelled flow. In a first order (or "flux-gradient") closure, the turbulence is approximated as being equivalent to an increased viscosity of the fluid. The second order closures parameterise higher order terms like redistribution, transport and dissipation.

4.1 K-theory and the Canopy Flow Model of Wilson et al (1998)

K-theory (i.e. first-order closure) relates the shear stress to the velocity gradient. In its full form, *K*-theory has correct tensor symmetry, i.e.

$$\overline{u_i' u_j'} = -K\left(\frac{\partial \overline{u}_i}{\partial x_j} + \frac{\partial \overline{u}_j}{\partial x_i}\right) \qquad (4.1)$$

where K is a turbulent transport coefficient, or eddy viscosity, which normally can take only positive finite values. The most familiar component $\overline{u'w'}$, which appears in the basic canopy flow equation, is given by

$$\overline{u'w'} = -K\left(\frac{\partial \overline{u}}{\partial z} + \frac{\partial \overline{w}}{\partial x}\right) \qquad (4.2)$$

K-theory represents turbulent convection by the unresolved scales as if it were a diffusive process. For horizontally uniform canopy flow Equation (4.2) simplifies to

$$\overline{u'w'} = -K\frac{\partial \overline{u}}{\partial z} \qquad (4.3)$$

Usually in first order closures the vertical transport of TKE is also parameterised as a diffusion process, viz.

$$PT_t = -\mu K \frac{\partial k}{\partial z}$$

W98 parameterise the eddy viscosity as $K = \lambda(z)\sqrt{c_e k(z)}$, where $\lambda(z)$ is an algebraic length scale; c_e is a constant representing the equilibrium shear-stress/TKE ratio (u_*^2 / k_0) immediately above the canopy; and k is the turbulent kinetic energy (TKE) calculated from the simplified transport equation. The diffusion coefficient for TKE, μK, is proportional to the eddy viscosity, with proportionality constant μ (following W98, we set $\mu = 0.2$).

4.1.1 Length Scale

Following W98 the length scale is characterised as the maximum of an *inner* and an *outer* length scale $\lambda = \max(\lambda_i, \lambda_o)$. The inner scale λ_i recognises the limitations to eddy size due to proximity to ground and the presence of the canopy. The outer scale λ_o recognises the displacement due to the canopy and, for the case of a wind tunnel experiment, a finite limiting value L_∞. These inner and outer scales are defined as

$$\frac{1}{\lambda_i} = \frac{1}{k_v z} + \frac{1}{\lambda_c} \qquad (4.4)$$

$$\frac{1}{\lambda_o} = \frac{1}{k_v (z-d)} + \frac{1}{L_\infty} \qquad (4.5)$$

where $k_v = 0.4$ is the von Kármán constant, and d is the displacement height (usually set as $\frac{2}{3}$ of the canopy height). W98 specify an upper limit λ_c to the *canopy* length scale as

$$\lambda_c = c\sqrt{k(h_c)}\left(\frac{\partial \overline{u}}{\partial z}\right)_{h_c}^{-1}, \qquad (4.6)$$

where c is an constant of proportionality, which W98 determined to be $c = 1.0$ as a reasonable approximation. Equation (4.6) is based on the suggestion of Raupach et al. (1996) that the strength of the wind shear at the canopy height is critical to eddy transport within a canopy. See Figure 4-1 for a length scale profile calculated for the Duke Forest.

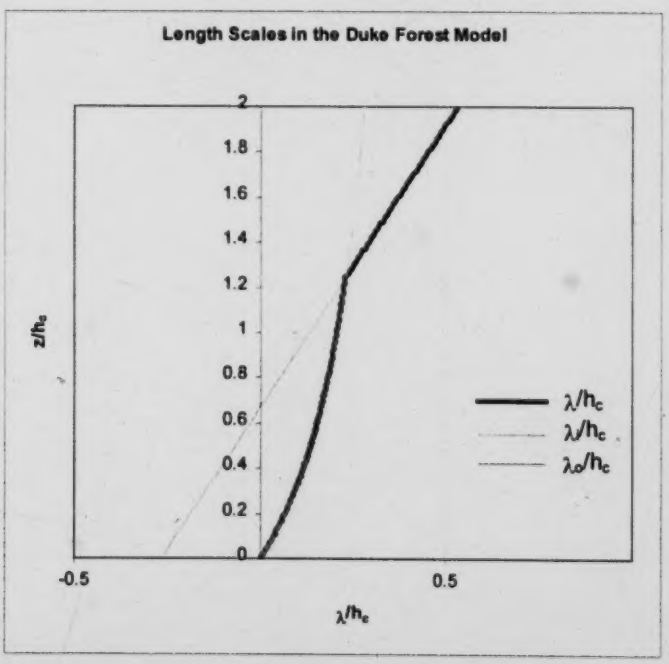

Figure 4-1: The K-theory closure introduces a turbulence length scale, whose height variation is shown here for the Duke Forest. The slope $\partial\lambda/\partial z = k_v$, in both limits $z \ll h_c$, and $z \gg h_c$.

4.1.2 TKE Dissipation Rate

Also known as viscous dissipation, it is the rate at which turbulent kinetic energy is converted into heat by doing work against viscous stress. It is written as $\varepsilon = \max(\varepsilon_{cc}, \varepsilon_{fd})$ where:

$$\varepsilon_{cc} = \frac{(c_\varepsilon k)^{3/2}}{\lambda} \text{ and } \varepsilon_{fd} = \alpha C_d a \overline{u} k .$$

The term ε_{cc} is a sink, which balances shear production of TKE in a local equilibrium layer far above the canopy. It is a standard parameterisation for viscous dissipation. The form drag ε_{fd} converts resolved TKE to small, rapidly dissipated "wake-scales". The closure constant α is reasoned by W98 to be $\alpha \approx 1$.

4.2 Higher-Order Closures

Higher-order closures appeal to the Navier-Stokes equations themselves to obtain exact governing equations for the turbulence statistics ($\overline{u_i' u_j'}$), which are subsequently simplified so as to attain closure (as many equations as unknowns). These equations are quite complex, and a single example will be given, that of the streamwise variance $\overline{u'^2} = \sigma_u^2$ in a flow with y-symmetry:

$$\begin{aligned} \frac{\partial \overline{u'^2}}{\partial t} + \overline{u}\frac{\partial \overline{u'^2}}{\partial x} + \overline{w}\frac{\partial \overline{u'^2}}{\partial z} = & -2\,\overline{u'^2}\frac{\partial \overline{u}}{\partial x} - 2\,\overline{u'w'}\frac{\partial \overline{u}}{\partial z} && \text{shear production} \\ & -\frac{\partial}{\partial x}(\overline{u'u'u'}) - \frac{\partial}{\partial z}(\overline{w'u'u'}) && \text{turbulent transport} \\ & -\frac{2}{\rho_0}\overline{u'\frac{\partial p'}{\partial x}} && \text{pressure transport} \\ & + \text{other terms} \end{aligned} \qquad (4.7)$$

Note that many mechanisms are resolved exactly by a second-order closure, e.g. advection of variance $\bar{u}\,\partial\overline{u'^2}/\partial x$ and the shear production of variance (e.g. $\overline{u'w'}\,\partial\bar{u}/\partial z$). Other mechanisms have to be approximated, for example the triple moments $\overline{u_i' u_j' u_k'}$ are often assumed to be fluxes driven by spatial gradients in $\overline{u_i' u_j'}$; an eddy diffusivity of second order (K^{2O}) is introduced, e.g.

$$\overline{w'u'u'} = -K^{2O}\frac{\partial\overline{u'^2}}{\partial z}. \qquad (4.8)$$

4.2.1 Wilson and Shaw (1977)

In their assumptions of steady state, horizontally-uniform, and neutrally-stratified flow in a canopy, WS77 developed a set of five equations representing the budgets for mean momentum, Reynolds stress, and the three components of the turbulent kinetic energy.

Momentum:

$$0 = -\frac{d\overline{u'w'}}{dz} - C_d a\,\bar{u}^2 \qquad (4.9)$$

Reynolds Stress:

$$0 = -\overline{w'^2}\frac{d\bar{u}}{dz} + 2\frac{d}{dz}\left[q\lambda_1\frac{d\overline{u'w'}}{dz}\right] - \frac{q}{3\lambda_2}\overline{u'w'} + Cq^2\frac{d\bar{u}}{dz} \qquad (4.10)$$

Variance of the longitudinal component:

$$0 = -2\overline{u'w'}\frac{d\overline{u}}{dz} + \frac{d}{dz}\left[q\lambda_1 \frac{d\overline{u'^2}}{dz}\right] + 2C_d a\,\overline{u}^2 - \frac{q}{3\lambda_2}\left[\overline{u'^2} - \frac{q^2}{3}\right] - \frac{2}{3}\frac{q^3}{\lambda_3} \qquad \textbf{(4.11)}$$

Variance of the lateral component:

$$0 = \frac{d}{dz}\left[q\lambda_1 \frac{d\overline{v'^2}}{dz}\right] - \frac{q}{3\lambda_2}\left[\overline{v'^2} - \frac{q^2}{3}\right] - \frac{2}{3}\frac{q^3}{\lambda_3} \qquad \textbf{(4.12)}$$

Variance of the vertical component:

$$0 = 3\frac{d}{dz}\left[q\lambda_1 \frac{d\overline{w'^2}}{dz}\right] - \frac{q}{3\lambda_2}\left[\overline{w'^2} - \frac{q^2}{3}\right] - \frac{2}{3}\frac{q^3}{\lambda_3} \qquad \textbf{(4.13)}$$

where $q = (\overline{u_i' u_i'})^{1/2} = \sqrt{2k}$ is a turbulent velocity scale, λ_1, λ_2, λ_3 are distinct length scales and are functions of z, and C is a constant. The five unknowns are $\overline{u}$, $\overline{u'w'}$, $\overline{u'^2}$, $\overline{v'^2}$, $\overline{w'^2}$.

4.2.2 Wilson (1988)

This model has a similar set of equations as WS77, but incorporates a dual frequency band for turbulent kinetic energy (TKE). In canopy flow, viscous and form drag on the vegetation cause a transformation of mean flow kinetic energy (MKE) to TKE, and a conversion of energy from the turbulent eddies to very small scale turbulent energy of the element wakes.

The low frequency band is "fed by" shear production. The turbulence time scale is taken to be the ratio k/ε between turbulent kinetic energy k in the low frequency band and its dissipation rate ε.

5 Numerical Method Used to Implement the K-Theory Model

For simulation of wind flow on level forested terrain, Equations (3.17) and (3.18) are discretised and solved using a computer programme written in C language.

5.1 SIMPLE: Discretisation with Respect to Control Volumes

The general procedure used here uses some aspects of the numerical method known as SIMPLE (Semi-Implicit Method for Pressure-Linked Equations), described by Patankar (1980). The governing equations are integrated across a control layer (see Figure 5-1) spanning height range $s \le z \le n$ to yield a "neighbour equation", linking velocity at the J^{th} grid point to its values above (J+1) and below (J-1). Our momentum equation, closed using K-theory, upon such integration gives:

$$\left[-K\frac{\partial \overline{u}}{\partial z}\right]_s^n = -\Delta z\, C_J\, \overline{u}_J^2 \qquad \textbf{(5.1)}$$

where the drag coefficient C_J is either $\overline{C_d}\, a(z)$, or $C_{dh} = \overline{C_d ah}$ (in the latter case Equation 5.1 takes a slightly different, and dimensionless, form). Numerical values for the drag coefficient were derived in Sections 3.5.2 and 3.5.3.

The momentum fluxes across the north (n) and south (s) faces are evaluated as

$$\left(K\frac{\partial \overline{u}}{\partial z}\right)_n = K_n \frac{\overline{u}_{J+1} - \overline{u}_J}{\Delta z} \qquad \textbf{(5.2)}$$

$$\left(K\frac{\partial \overline{u}}{\partial z}\right)_s = K_s \frac{\overline{u}_J - \overline{u}_{J-1}}{\Delta z} \qquad \textbf{(5.3)}$$

By the same method the TKE budget equation can be discretised as

$$\left[-\mu K\frac{\partial k}{\partial z}\right]_s^n = -\Delta z\,\varepsilon - K\frac{\partial \overline{u}}{\partial z}\frac{\partial \overline{u}}{\partial z}\Delta z$$

The resulting neighbour equation for velocity is

$$-A_n^u\,\overline{u}_{J+1}^m + A_c^u\,\overline{u}_J^m - A_s^u\,\overline{u}_{J-1}^m = \Delta z\left(-\frac{1}{\rho_0}\frac{\partial \overline{p}}{\partial x}\right)_J \qquad \textbf{(5.4)}$$

where

$$A_n^u = \frac{K_n}{\Delta z}, \qquad A_s^u = \frac{K_s}{\Delta z}, \qquad A_c^u = A_n^u + A_s^u + \Delta z\,C_d a h_c\left|\overline{u}_J^{m-1}\right|$$

and where superscript m designates the m^{th} (iterative) guess for the $\overline{u}$ field.

For the TKE equation we obtain

$$-A_n^k\,k_{J+1}^m + A_c^k\,k_J^m - A_s^k\,k_{J-1}^m = \Delta z\,\lambda\sqrt{c_\varepsilon k}\left(\frac{\partial u}{\partial z}\right)^2 \qquad \textbf{(5.5)}$$

where

$$A_n^k = \mu\frac{K_n}{\Delta z}, \quad A_s^k = \mu\frac{K_s}{\Delta z}, \quad A_c^k = A_n^k + A_s^k + \Delta z\max\left(\frac{\sqrt{c_\varepsilon k_J^{m-1}}}{\lambda}, \alpha C_d a\left|\overline{u}_J^{m-1}\right|\right)$$

In combination, difference Equations (5.4, 5.5) express conservation in each control layer described in the following section.

5.2 Staggered Grid

The grid (see Figure 5-1) is staggered in such way that the odd velocity moments $\overline{u}$ (and pressure gradients in wind tunnel experiments) are defined at grid points offset relative to the even moments, notably Reynolds stress $\overline{u'w'}$ and TKE. The odd moment grid starts at the ground level with $\overline{u} = 0$ and the even moment grid is set half a grid spacing up with the uppermost grid point at $z = Z_{max}$.

With this procedure, grid points yield a set of N simultaneous algebraic equations in N unknowns ($\overline{u}_1 \ldots \overline{u}_J \ldots \overline{u}_N$) that are solved using a tri-diagonal matrix solver built in the standard algebraic software (Press, 1988).

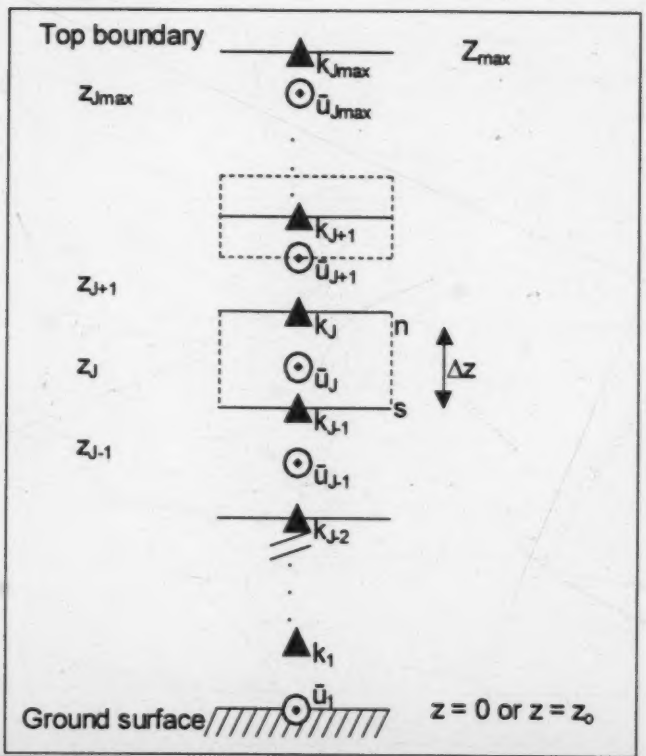

Figure 5-1: Control volumes and grid point layout for discretised model. There are two staggered grids: one has the odd moment $\overline{u}$ and the other has the even moments $\overline{u'w'}$ and k. The grid spacing Δz is uniform.

5.3 Boundary conditions

5.3.1 Top

The top of the model is placed at 10 h_c for all simulations. The upper boundary condition for the u-momentum equation is a prescribed value (-1) for momentum influx $\overline{u'w'}/u_*^2$. For TKE, the top boundary condition in open atmospheric flow is a prescribed equilibrium value ($1/c_\varepsilon$) for k/u_*^2. In the case of a wind tunnel simulation, we set $\partial k/\partial z = 0$ at the upper boundary.

5.3.2 Bottom

At the bottom boundary, the mean wind speed at the ground ($z = 0.0$) is $\overline{u} = 0$, and we imposed $\partial k/\partial z = 0$ (flux of TKE to ground vanishes).

5.4 Investigation of Model Convergence and Grid-Independence

In a grid-based, iterative numerical wind flow model, it is necessary to seek an adequately refined spacing of grid points, and an adequate number of iterations. To systematically study these issues we focused on the Furry Hill experiment, described in W98.

5.4.1 Grid Size Optimisation

Several runs were made at various numbers of grid points in the canopy. All other variables were held constant including the number of iterations, which was 200

for this case as was used in the W98 simulations. Results are shown in Figure 5-2 and Figure 5-3.

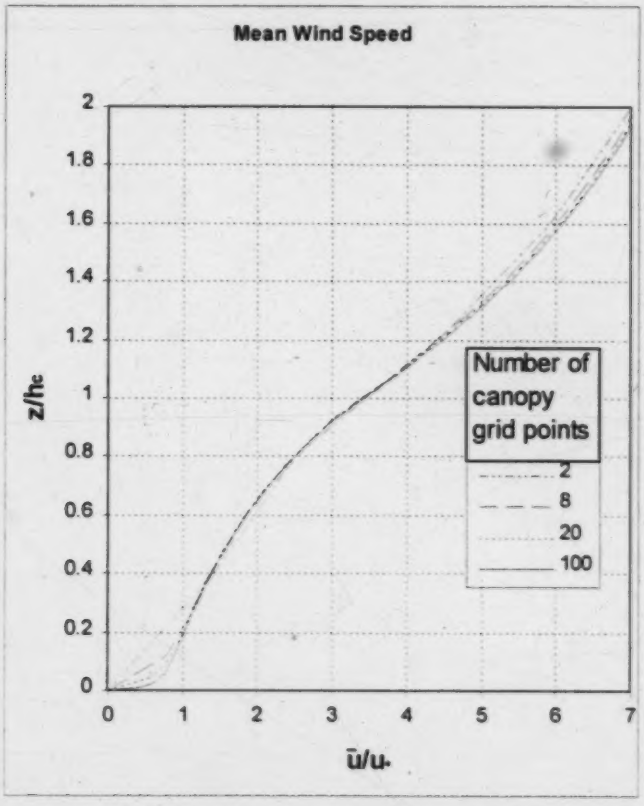

Figure 5-2: Sensitivity of modelled profile of mean wind to grid spacing. Shows change in curve shape with increase in number of vertical grid points in the model. The grid point numbers represent the number of "full boxes" within the canopy.

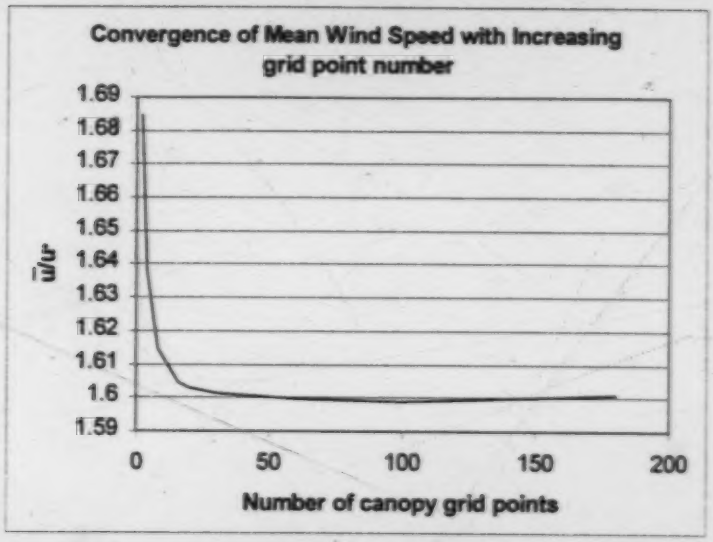

Figure 5-3: Using mean wind speed values at height $z/h_c = 0.5$ from Figure 5-2 above, this figure shows how increasing the number of vertical grid points levels converges the simulation.

5.4.2 Iteration number Optimisation

The next test seeks the minimum number of iterations that is needed to achieve a reasonable equilibrium in the model. Comparisons show the number of iterations for convergence. Figure 5-4 shows the shape of the wind speed profile in the Furry Hill forest. Figure 5-5 shows the mean wind speed at a height halfway up the canopy. It can be seen that the model converges at approximately 50 iterations.

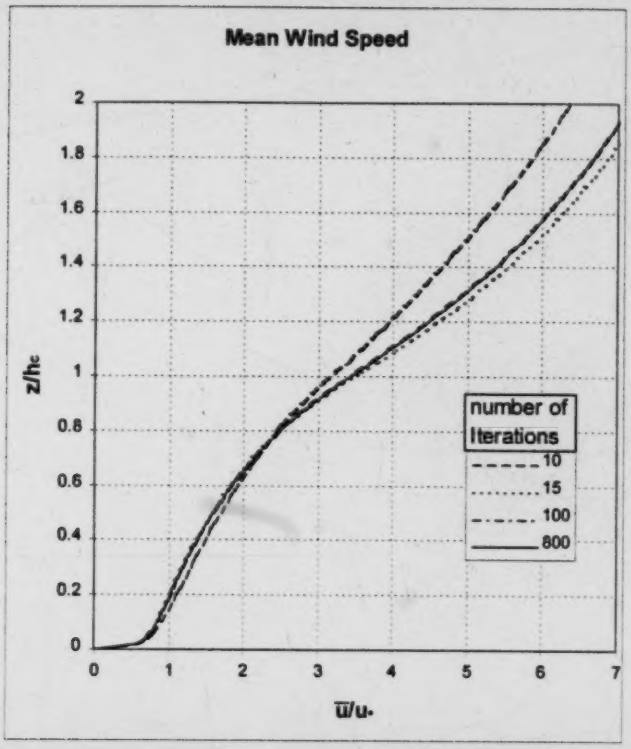

Figure 5-4: The normalised mean wind profile with 100 grid points in the canopy. The heavier line in the graph represents the iteration numbers 100, and 800.

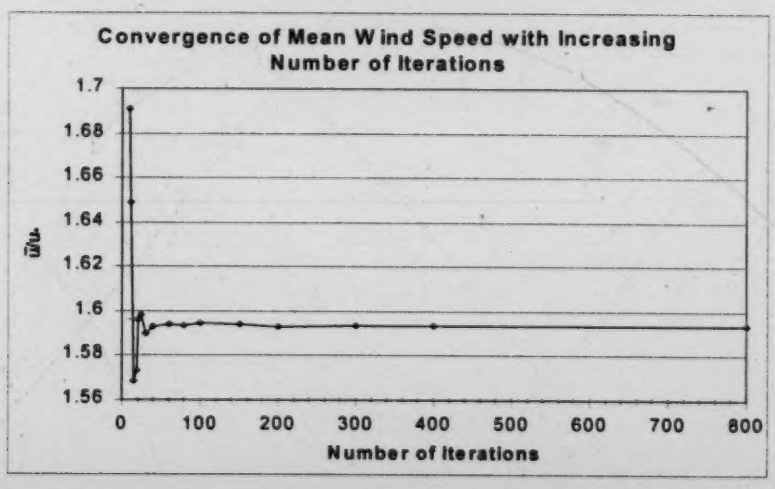

Figure 5-5: More specific depiction of convergence in speed values taken at height halfway up the canopy. This shows that the simulation converges at 300 iterations, but good results are accomplished after about 50 iterations.

6 Comparison of Numerical with Experimental Data and with Others' Calculations

The numerical wind and turbulence model described in Section 4.1 is a first-order closure model, that will now be compared to more complex (second order) closure models, and to observations from four experimental flows, known as the Tombstone Canopy; Furry Hill; the Elora Corn Canopy; and the Duke Forest.

The Tombstone Canopy (Raupach et al. 1986) was an array of vertical bars, each 6 cm high by 1 cm in cross-stream width, these being arranged in a regular diamond pattern, with 6 cm cross-stream and 4.4 cm along-stream spacing, on the floor of a wind tunnel.

Furry Hill was also a wind tunnel flow experiment, but in this case the plant canopy was flexible, having been constructed with strands of fishing line fixed in a base, and standing 0.47 cm high.

The Elora experiments took place in a 2.2-m high mature corn canopy, growing at Elora, Ontario, and normalised velocity and turbulence profiles were built up by pooling measurements made in a range of conditions, from two specially-constructed, servo-controlled split-film anemometers (one served as reference at $z = h_c$; the other was shifted along the vertical axis to build up a "map" of the normalised profiles).

As earlier stated, the Duke Forest was a 14-m loblolly pine canopy, in North Carolina.

In all simulations the number of grid points in the canopy was set at 100, or $\Delta z/h_c = 0.01$, and the number of iterations for convergence was set at 100.

6.1 Revisiting and Independently Checking the Wilson et al. (1998) first order closure model

To increase confidence both in my own simulations and in those carried out by W98, their simulations of the Furry Hill, Elora Corn, and Tombstone Canopy flows were repeated. Results are given on Figure 6-1, Figure 6-2, and Figure 6-3 , and these must be compared to the corresponding figures in W98. All three simulations use $c = 1.0$, $\alpha = 1.0$, and $\mu = 0.2$ (i.e. no change from W98).

The model simulations for Furry Hill (Figure 6-1) and Elora (Figure 6-2) compared well with W98. The only difference between our simulations and W98 is in the number of vertical grid points specified within the canopy layer. In the simulations by W98, twenty vertical grid points were used for Furry Hill and the Tombstone Canopy, but only ten grid points for the Elora Corn. Here I have used one hundred (100) grid points in simulations of the three canopies. This refinement has not revealed any visually significant improvement over the W98 simulations.

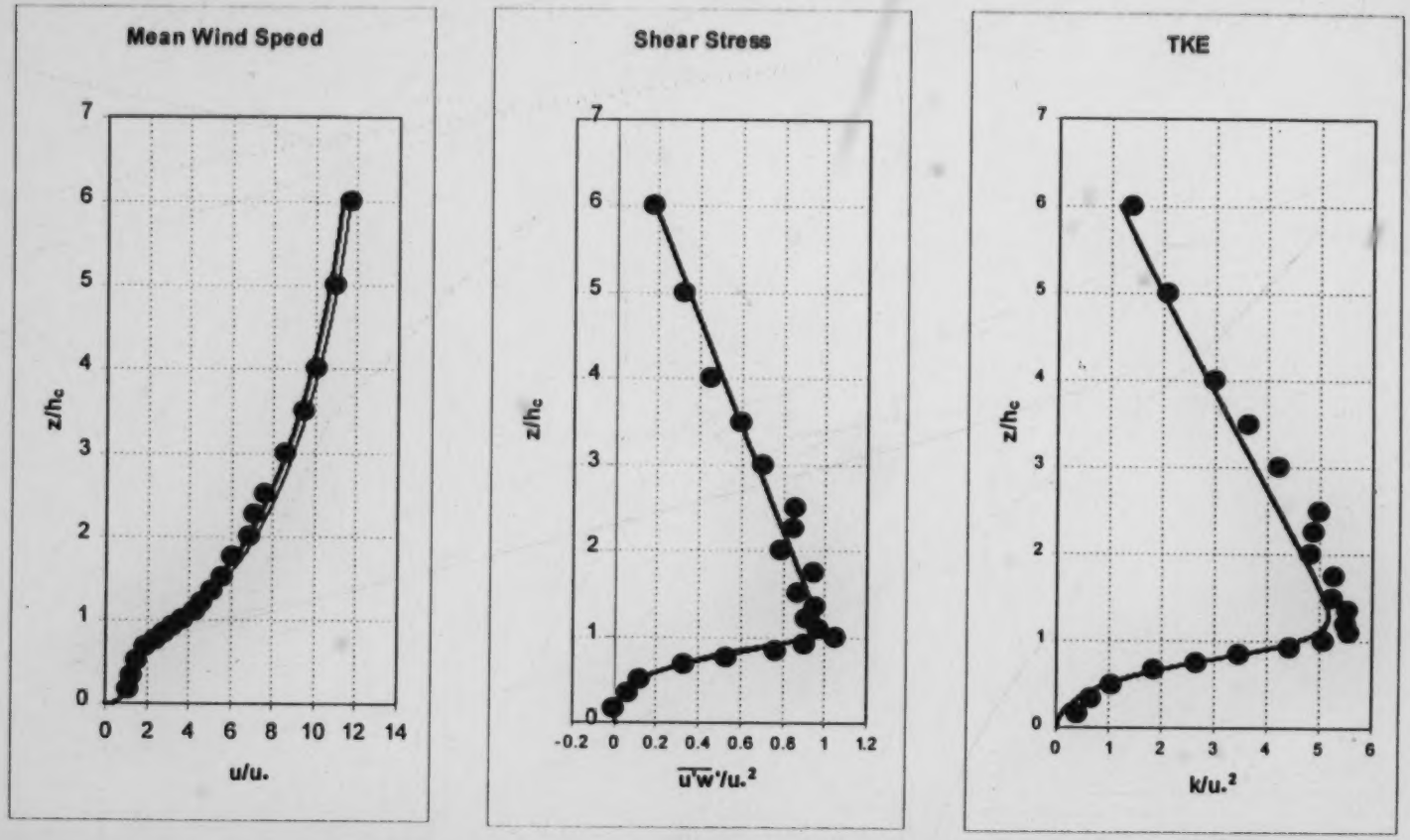

Figure 6-1: New simulations (with first-order closure) for the Furry Hill Experiment (i.e. a check on results of Wilson et al 1998). The thin line represents bulk $C_{db} = C_d a h_c = 0.32$. The thick line represents height-variable $\overline{C}_d a h_c$.

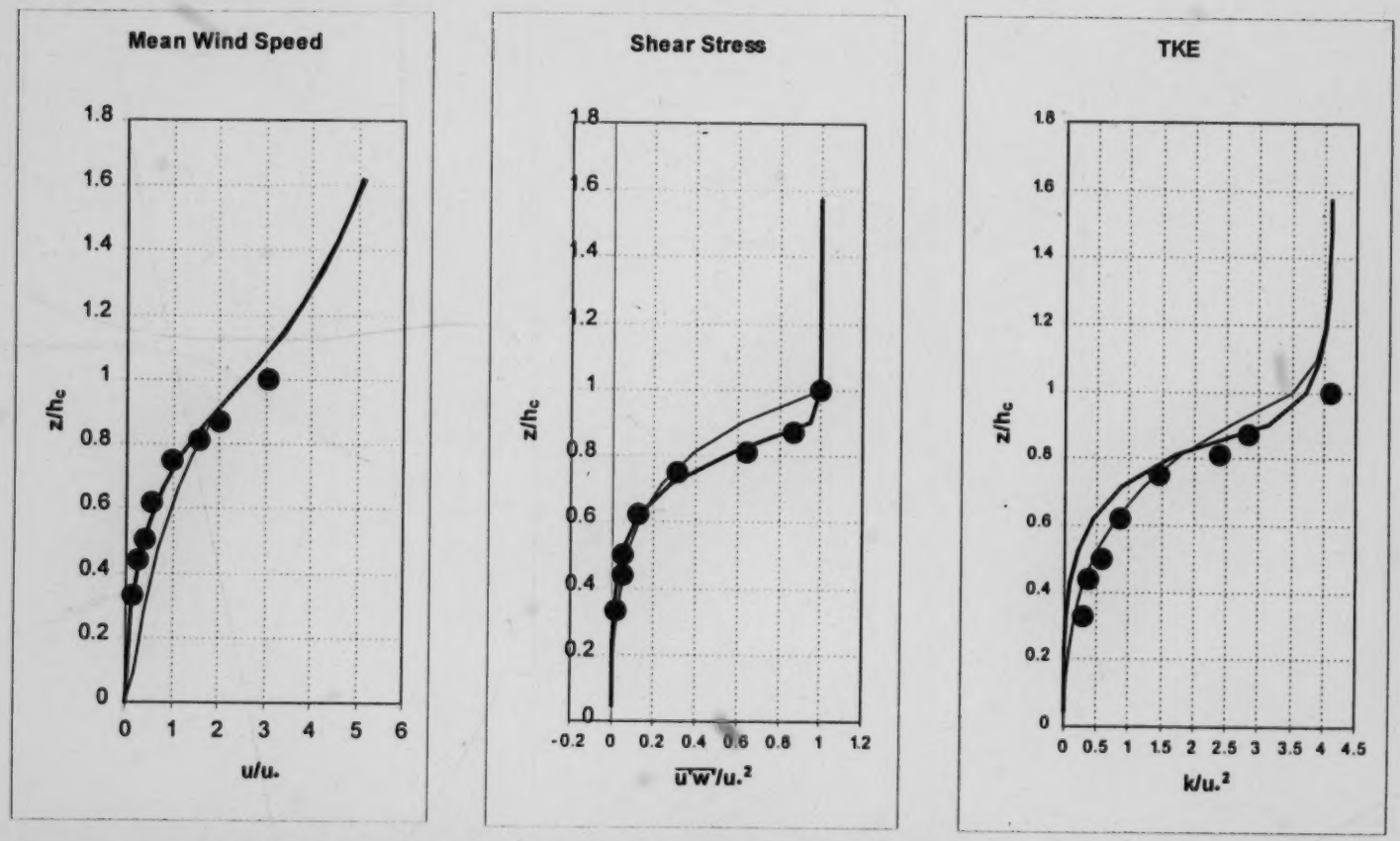

Figure 6-2: New simulations (with first-order closure) for the Elora maize (i.e. a check on results of Wilson et al 1998). The thin line represents bulk $C_{db} = C_d a h_c = 0.79$. The thick line represents height-variable $\overline{C_d a h_c}$.

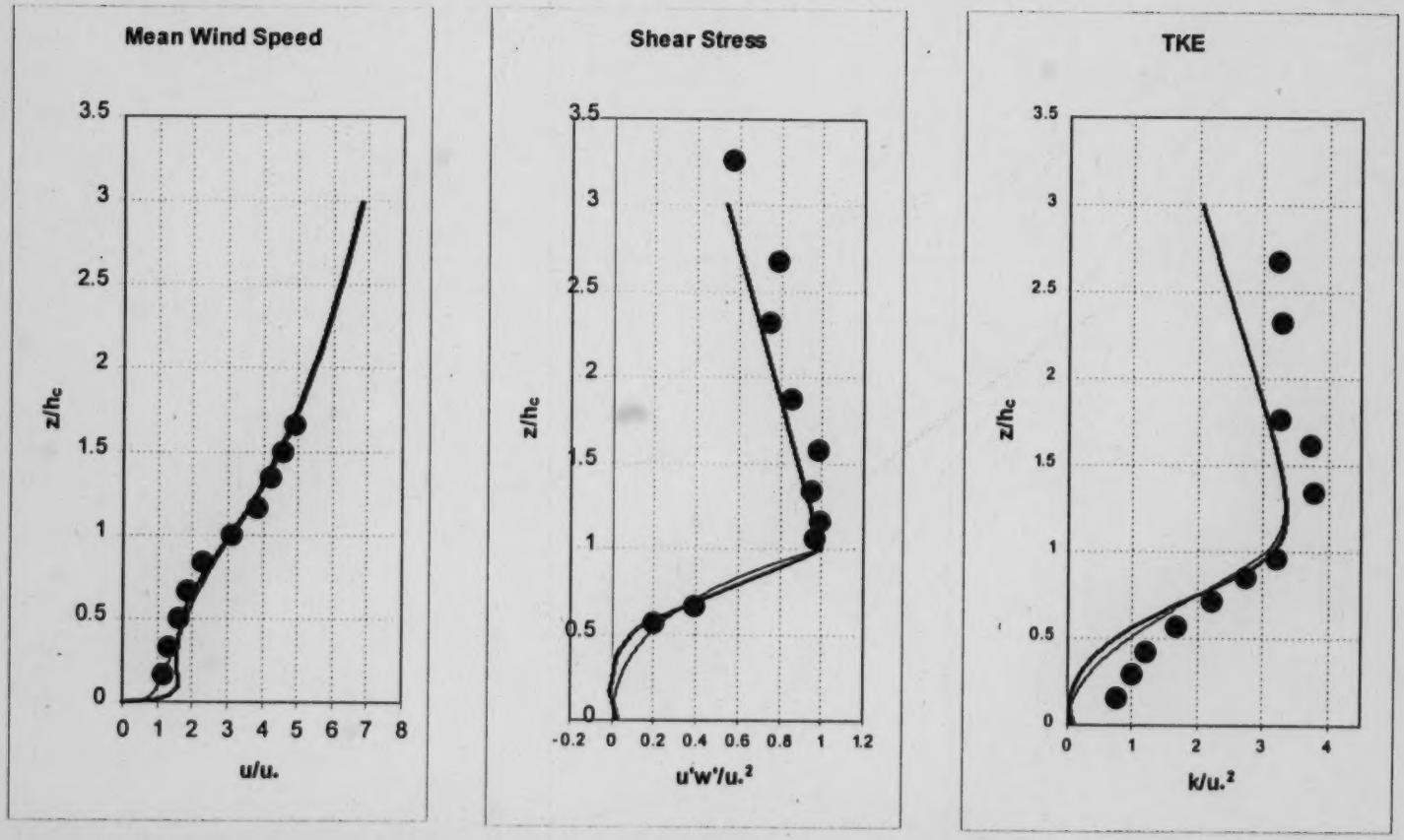

Figure 6-3: New simulations (with first-order closure) for the Tombstone canopy (i.e. a check on results of Wilson et al 1998). The thin line represents bulk $C_{db} = C_d a h_c$=0.31. The thick line represents height variable $\overline{C_d a h_c}$.

In the case of the Tombstone simulation, where we used a variable drag coefficient, the mean wind speed profile showed an increase in speed at $z/h_c < 0.4$. This is different to the W98 simulation, presumably due to the refined grid used here. Another difference related to the earlier simulations, which our refined grid revealed, is the shear stress, which becomes negative from $0.12 < z/h_c < 0.21$. The TKE profile becomes much less than the measured profile below $z/h_c < 0.5$ (It is zero in the range $0.06 < z/h_c < 0.16$). This simulation outcome is probably a result of the drag coefficient having been set to zero from the ground to approximately $z/h_c = 0.16$, which is unrealistic since a plant canopy must be attached to the ground and have a non-vanishing plant area density in the entire range $0 \le z \le h_c$.

I further experimented with the Tombstone simulation by modifying the drag coefficient profile to ensure continuity from the main plant canopy to the ground. I used $\overline{C_d}ah_c = 0.18$ from $z/h_c = 0.16$ and applied it to all values for range $z/h_c \le 0.16$. The new simulation is shown in Figure 6-4. It shows some improvement in the mean wind profile at $z/h_c \le 0.3$. The shear stress profile shows no negative values. There is, however, no marked improvement in the the TKE profile.

Having seen satisfactory agreement of our simulations with those of W98, we may now move on and compare the first-order closure model against observations and second-order simulations of the Duke Forest flow, which were given by KC99.

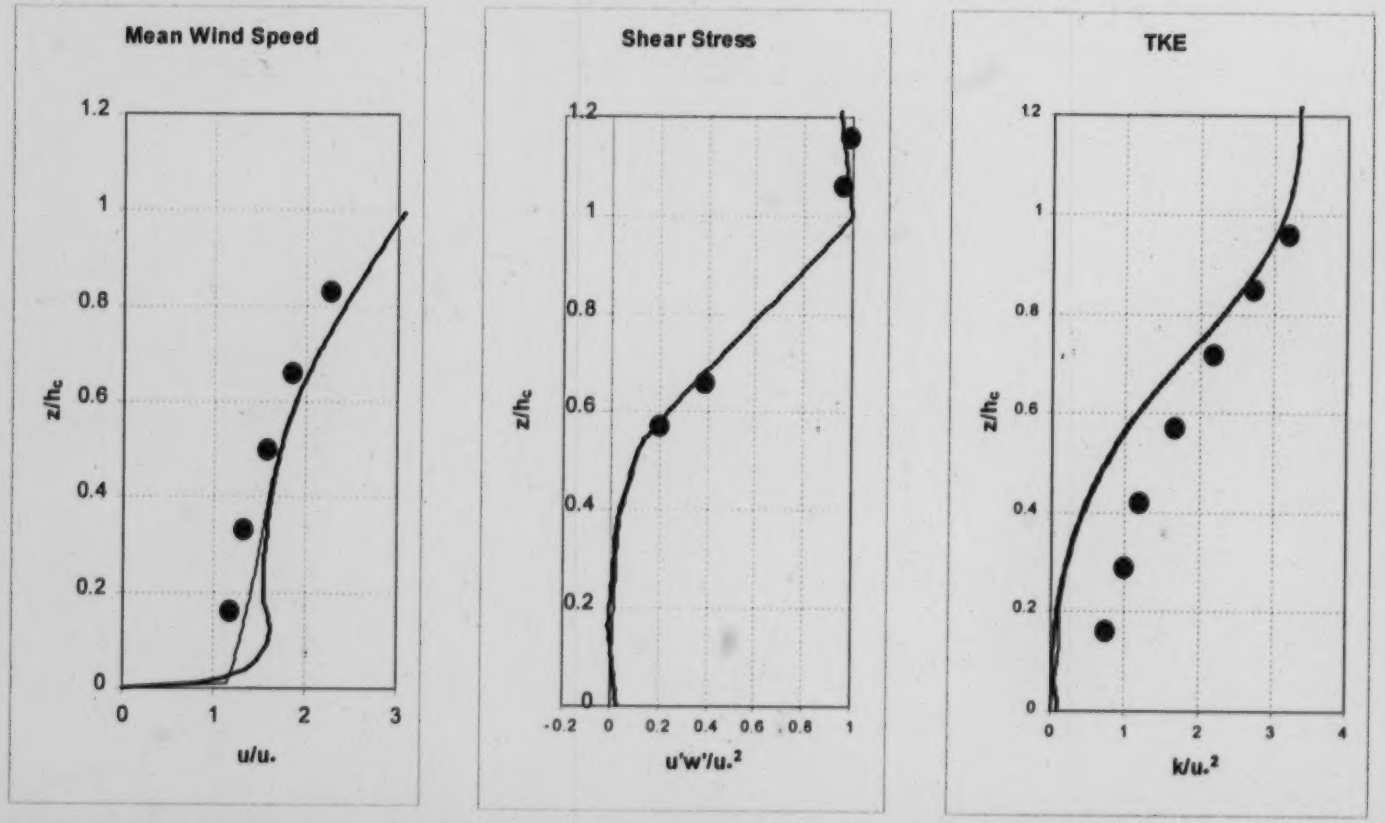

Figure 6-4: In the original Wilson et al (1998) simulation of Tombstone the variable $\overline{C}_d a h_c$ was 0.0 at $z/h_c \leq 0.16$ (thick solid line). A new simulation setting $\overline{C}_d a h_c = 0.18$ for $z/h_c \leq 0.16$ is shown as a thin line and shows some improvements in the mean wind profile. The shear stress profile shows no negative values.

6.2 Comparing the First Order Model to Duke Forest Observations and Simulations from Katul and Chang (1999)

Because our objective is to assess the relative merits of our own first-order model against the second-order models examined by KC99, in our application of the first-order closure model to Duke Forest, we follow KC99 as closely as possible. The top of the model domain was chosen as 10 times the canopy height h_c. As derived in Sections 3.5.2 and 3.5.3, the height averaged drag coefficient (for use in conjunction with the measured profile of leaf area density) was $\overline{C_d} = 0.2$, while for simulations using a bulk drag coefficient, we set $C_{db} = 0.34$. The zero-plane displacement height $d/h_c = 0.67$. The number of grid points in the canopy and the number of iterations are both 100, which is known to be adequate from results in Section 0. The normalised standard deviations for perturbations u', v', w' are respectively, 2.08, 1.86, and 1.22 as reported by KC99 for z/h_c =1.097, i.e. just above the canopy. The parameters for Duke Forest are shown in the parameter list of Table 6-1.

Table 6-1: Parameters of the Duke Canopy Experiments

Property	Symbol	Value
Canopy height	h_c	14.0 m
Model Height	Lid	10 h_c
Bulk drag parameter calculated in Section 3.5.3	$C_{db} = \overline{C_d a}\, h_c$	0.34
Height averaged drag coefficient from Section 3.5.2 and as KC99	$\overline{C_d}$	0.2
Displacement height	d/h_c	0.67
Equilibrium variances as given by KC99	$\sigma_{u,v,w}/u_{*0}$	2.08, 1.86, 1.22
Closure coefficients	ϵ, α, μ	1.0, 1.0, 0.2
Limit to length scale	L_∞	1.5
Grid points/Iterations		100/100

Figure 6-5, Figure 6-6, and Figure 6-7 below show results of our simulation of the Duke Forest of KC99. Three variables, the mean wind speed $\overline{u}$, shear stress ($\overline{u'w'}$), and the turbulent kinetic energy (k) are compared in two simulations: one based on using the height-averaged drag coefficient in conjunction with the (measured) profile of leaf area density, and the other with the bulk drag coefficient. The two second-order simulations of KC99, namely WS77 and W88, have been overlaid onto the present (first-order) results, for easy comparison.

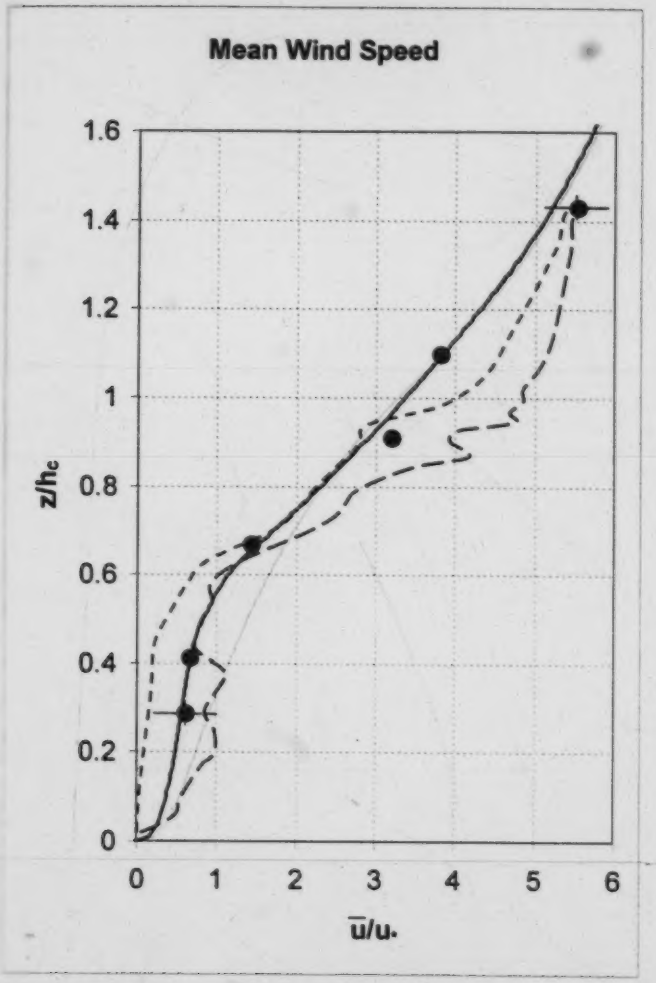

Figure 6-5: Mean wind speed $\overline{u}$ of the first order model against observed (•). These values are normalised to the friction velocity u_*. The height z is normalised to the height of the canopy h_c. The thick solid line is first-order closure with height averaged $\overline{C_d}$ = 0.2, the thin solid line is with a bulk C_{db} = 0.34. The long dashed line is W88, the short dashed line is WS77 as simulated by KC99.

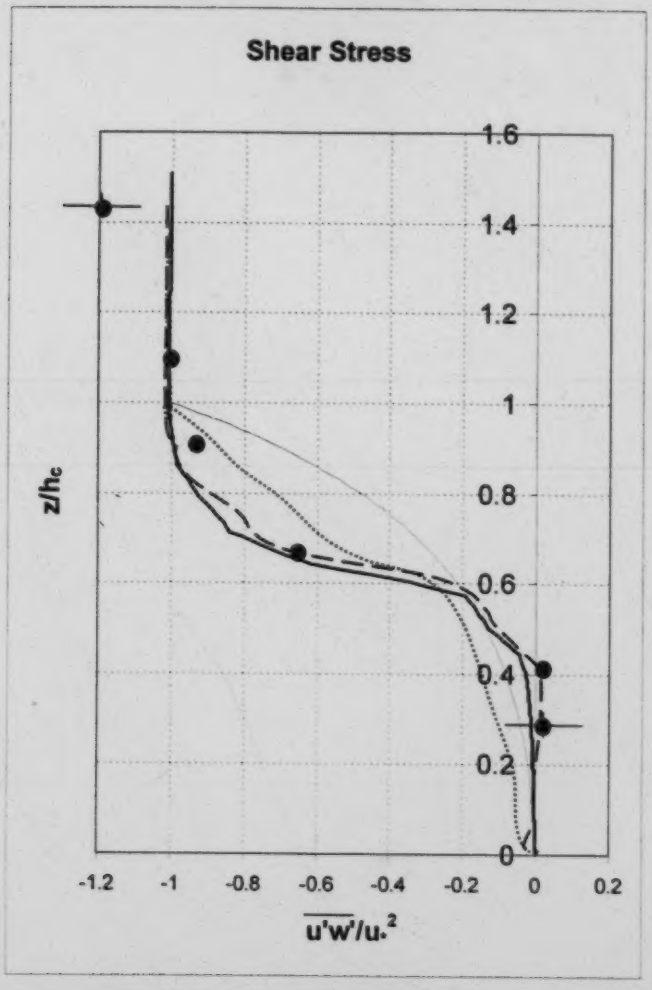

Figure 6-6: The shear stress $\overline{u'w'}$, from the first order model against observed (•). These values are normalised to the friction velocity u_*. The height z is normalised to the height of the canopy h_c. The thick solid line is first-order closure with height averaged $\overline{C_d}$ = 0.2, the thin solid line is with a bulk C_{db} = 0.34. The long dashed line is W88, the short dashed line is WS77 as simulated by KC99.

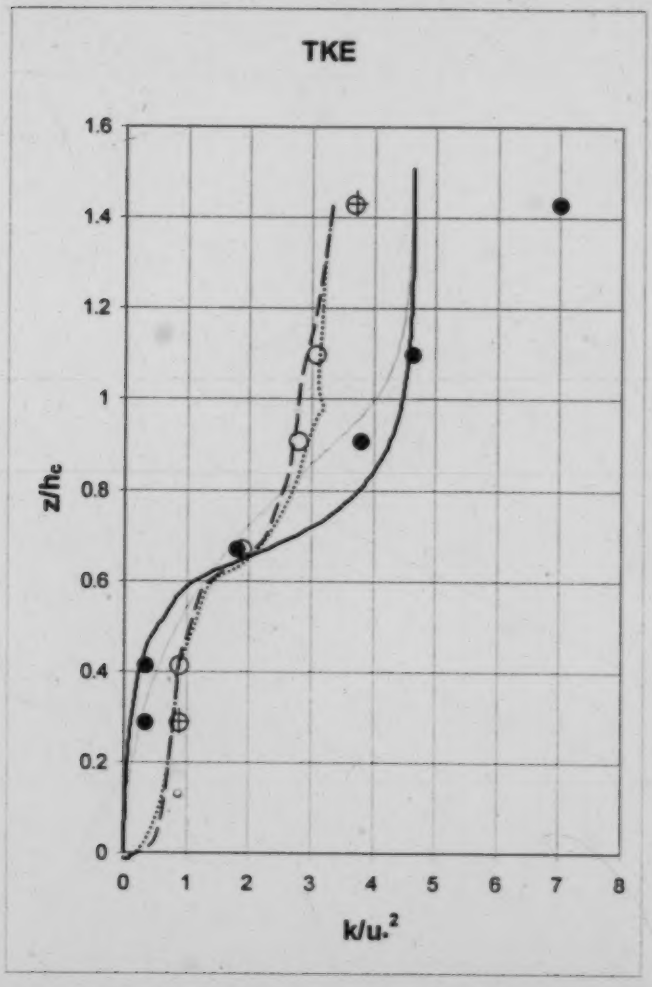

Figure 6-7: The turbulent kinetic energy k of the first order model against observed (•). The dot symbols (•) are the TKE recalculated from σ_u, σ_v, and σ_w given by KC99. The hollow symbols are TKE given by KC99. These values are normalised to the friction velocity u_*. The height z is normalised to the height of the canopy h_c. The thick solid line is first-order closure with height averaged $\overline{C_d} = 0.2$, the thin solid line is with a bulk $C_{db} = 0.34$. The long dashed line is W88, the short dashed line is WS77 as simulated by KC99. Note that our specification $c_\varepsilon = \left(k/u_*^2\right)_{hc}^{-1} = 4.64$ require our modelled k-profile to run through the observation at $z/h_c \approx 1$.

Figure 6-5 shows that our normalised mean wind speed profile using the height-averaged drag coefficient ($\overline{C_d}$) closely matches the observed profile of KC99, whereas our simulation using a bulk drag coefficient, while equally satisfactory well *above* the canopy, is seriously in error within the canopy. A good simulation using height-averaged $\overline{C_d}$ is not very surprising, since we derived that drag coefficient with reference to the actual (true) profiles of mean wind and shear stress. It should be expected, then, that the models should reproduce the mean wind and shear stress observations quite well (this is an admission with respect to these types of modelling exercises that is rarely made; but if one has fitted the coefficients of a model to a certain set of data, viz. in our case the drag coefficient, then one is hardly entitled to crow if the model then simulates those same data quite nicely). In any case, if on the basis of Figure 6-5 we are to say that the models are "good," then it is quite evident that the second-order models are not as "good" as the first-order model!

In the case of the normalised shear stress profile (Figure 6-6), our first-order model (using $\overline{C_d}$) also closely matches the measured values of KC99, except near $z/h_c = 1.4$; the simulation using a bulk drag coefficient gives a poor stress profile in the canopy. Our modelled stress profile (based on $\overline{C_d}$) is similar to that obtained by KC99 using the W88 model. A closer examination would indicate that one cannot simultaneously do a good job of the mean wind and a bad job of the shear stress – for it is implied by the way in which the drag coefficient is derived, that the modelled mean wind and shear stress **must** be consistent.

Figure 6-7 reveals some confusion with regard to the "real" normalised TKE profile. As stated earlier in Section 1.2 we found a discrepancy between our

recalculated TKE and the values shown in Figure 1 of KC99, (also shown in our Figure 1-1 and the reproduction of their Figure 1 in our Figure 6-8). Our first-order model follows our recalculated profile of the experimental TKE rather nicely.

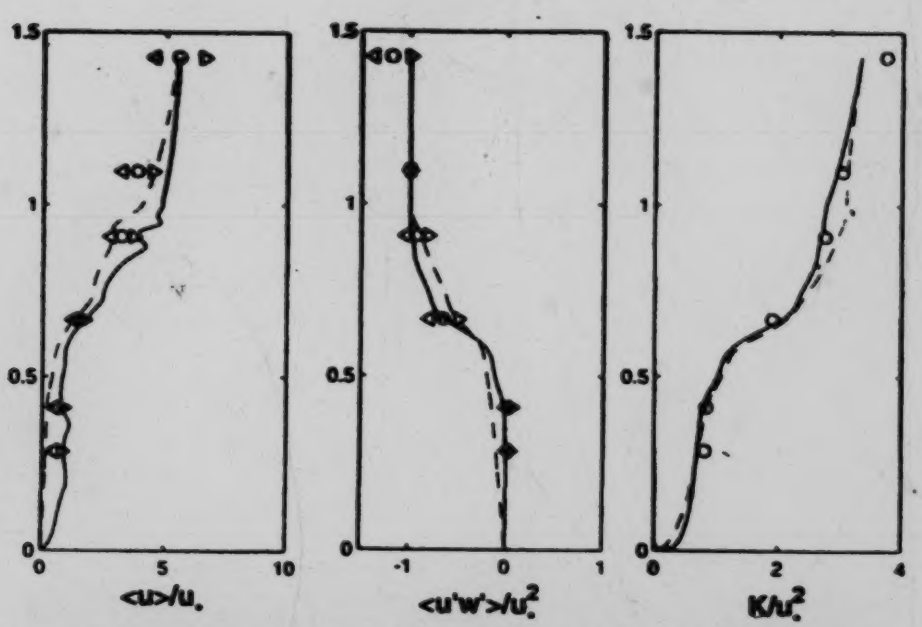

Figure 6-8: Reproduced from KC99 these are their charts of their modelled and observed normalised mean (here the brackets <> represent time averaged) wind speed, shear stress and turbulent kinetic energy (TKE = *K*). This series can be compared to our Figure 6-5, Figure 6-6, and Figure 6-7.

7 Conclusions

In this thesis I have studied a pre-existing first-order closure model for the simulation of wind and turbulence in a plant canopy. My original contributions relative to earlier reports on the model (Wilson et al., 1998; Wilson and Flesch, 1999) are:

1) Critical assessment of the means by which a drag coefficient is determined for a forest flow, and emphasis that, in common practise, wind models are "tuned" with respect to (i.e. not "independent" of) the very flow measurements they purport to describe.
2) Systematic study of requirements for grid independence and convergence (numerical issues).
3) Repeated the application of the model to the three diverse wind flows studied by W98, to confirm the consistency of my simulations with theirs.
4) Model application to simulate the Duke Forest wind flow reported by Katul and Chang (1999) with a specific focus on the question of how well the first-order model performs relative to second-order closures.

Simulations that do not discard information on the forest area density profile, but which use the height-averaged drag coefficient, were found to be the best choice (versus using either the bulk drag coefficient or the height-dependent drag coefficient). It was found that the height-dependent drag coefficient was difficult to calculate in light of the inevitably noisy wind shear data deep in a canopy, and that the bulk drag approach offered a poor representation of the (actually) highly variable leaf area density in the Duke Forest canopy.

From contributions 2) and 3), my findings show that W98 could have increased the number of grid points within their canopy simulations from 10

(Tombstone) and 20 (Furry Hill, Elora) to 100. This would have revealed some minor inconsistencies, such as the unrealistically low (zero) value imposed for the drag coefficient near the ground, in the Tombstone canopy.

Regarding the fourth and most significant contribution, I have shown a successful simulation of a flow through the Duke Forest using the first-order K-model $K \propto \lambda\sqrt{k}$. This has proven our hypothesis that a simpler model with fewer ambiguities can simulate the fundamental wind properties (mean wind speed, mean shear stress, and turbulent kinetic energy) quite as well as a second-order closure. That is, a second-order model is evidently not necessary to simulate the mean wind speed, shear stress and TKE profiles adequately well.

The observed TKE profile in Katul and Chang (1999) is puzzling in that it does not match our recalculated profile using their wind variance data. It is especially worrying that their simulations using the two second-order models match their (we think, bad) TKE profile very well.

A logical peculiarity of all of these wind flow simulations (both in my thesis, and in W98 and KC99) is that the drag coefficient, a key input, has been deduced from the very observations that the model is supposed to simulate. I have demonstrated the difficulty of deriving the drag coefficient, even given detailed flow observations – then one may well imagine how much the more so will C_d be uncertain, if it has to be prescribed only on the qualitative basis of specified forest "type" (boreal forest; deciduous forest; corn crop; etc…). The implication is that the theoretical superiority of a second-order model is rather moot, in the face of the large uncertainty with respect to the canopy drag coefficient that will ordinarily prevail, in any routine application of these types of models.

8 References

Holton, J.R., 1992, " An Introduction to Dynamic Meteorology." Academic Press Limited, London.

Justus, C.G., 1978, "Winds and Wind System Performance", The Franklin Institute Press, Philadelphia, Pennsylvania.

Kaimal, J.C., J.J. Finnigan, 1994, "Atmospheric Boundary Layer Flows: Their structure and measurement", Oxford University Press, New York.

Katul, G. G., Wei-han Chang, 1999, "Principal Length Scales in Second-Order Closure Models for Canopy Turbulence." Journal of Applied Meteorology: Vol. 38, No. 11, pp. 1631–1643.

Patankar, S.V., 1980: "Numerical heat transfer and fluid flow." Hemisphere Publication Co., London, UK.

Paulson, C.A., 1970, "The Mathematical Representation of Wind Speed and Temperature Profiles in the Unstable Atmospheric Surface Layer", Journal of Applied Meteorology. 9, 857-861.

Pielke, R.A., 1984, "Mesoscale Meteorology Modelling." Academic Press, Inc., San Diego, CA, USA.

Press, W.H., B.P. Flannery, S.A. Teukolsky, W.T. Vetterling, 1988, "Numerical Recipes in C: The Art of Scientific Computing." Cambridge University Press, New York, NY, USA.

Raupach, M.R., Finnigan, J.J., and Brunet, Y., 1996, "Coherent eddies and turbulence in vegetation canopies: the mixing-layer analogy." Boundary-Layer Meteorology, 78, 351-382.

Raupach, M.R., Shaw, R.H., 1982, "Averaging Procedures for Flow Within Vegetation Canopies", Boundary Layer Meteorology, **22**, 79-90.

Shinn, J.H., 1971, "Steady-state two-dimensional airflow in forests and the disturbance of surface layer flow by a forest wall." Ph.D. Thesis, University of Wisconsin, Madison, 91pp.

Wilson, J.D., 1988: "A second-order closure model for flow through vegetation." Boundary-Layer Meteorology, **42**, 371-392.

Wilson, J.D., T.K. Flesch, 1999: "Wind and remnant tree sway in forest cutblocks. III. a windflow model to diagnose spatial variation." Agricultural and Forest Meteorology, **93**, 259-282.

Wilson, J. D., J.J. Finnigan, and M.R. Raupach, 1998: "A first-order closure. For disturbed plant canopy flows, and its application to windflow through a canopy on a ridge." Quarterly Journal of the Royal Meteorological Society, Vol. 124, pp 705-732.

Wilson, N. R., R. H. Shaw, 1977: "A higher order closure model for canopy flow." Journal of Applied Meteorology, **16**, 1197-1205.